VEIN FORMATION IN RELATION TO BURIAL DIAGENESIS IN THE MIOCENE MONTEREY FORMATION, ARROYO BURRO BEACH, SANTA BARBARA, CALIFORNIA

Peter Eichhubl
Department of Geological and Environmental Sciences, Stanford University, CA 94305

James R. Boles
Department of Geological Sciences, University of California, Santa Barbara, CA 93106

ABSTRACT

Four distinct generations of veins are observed at Arroyo Burro Beach, each representing repeated episodes of fracture opening and cementation. The first set of dolomicrite veins formed during early burial in the zone of microbial methanogenesis, based on the heavy $\delta^{13}C$ composition of dolomite cement. The second vein set, cemented by quartz, apparently accompanied opal-CT dissolution and quartz precipitation in the siliceous dolostone host rock. The third vein generation, forming dolomite cemented breccias, correlates with recrystallization of dolomite pore cement in the host rock. The fourth set of calcite veins partly reactivates earlier vein generations, but is most extensively developed adjacent to mesoscale faults. Calcite veins are characterized by their clustered occurrence, with the formation of subparallel veins ultimately leading to host rock fragmentation and to breccia-filled veins. Carbonate dissolution in the host rock and the precipitation of carbonate vein cement may be related to organic matter diagenesis and incipient catagenesis leading to release of organic acids into the pore fluid. Enhanced diagenetic alteration of host rock fragments in all vein generations suggests that fractures served as catalysts for diagenetic reactions, presumably by opening the system to mass transfer and by increasing the water-rock ratio.

INTRODUCTION

In sedimentary sequences, diagenesis, deformation, and fluid flow are mutually dependent processes: Diagenesis may release pore fluid through dehydration reactions which may lead to an increase in pore fluid pressure and thus to brittle deformation by the formation and reactivation of faults and extension fractures. Faults and fractures provide pathways for fluid flow and mass transfer thus promoting diagenetic reactions. Diagenetic processes, on the other hand, such as cementation, recrystallization, and dissolution, affect the rheologic response of rocks to deformation, thus controlling fracture formation and folding. Cementation, for instance, may increase the susceptibility of a rock layer to fracturing. In addition to altering rock rheology, diagenetic reactions may also affect fracture formation by changing the local stress state. The stress state could be affected by changes in pore fluid pressure through dehydration reactions or by dissolution or replacement of the load-supporting solid framework. Diagenetic changes in stress state are likely to be superposed over changes in basin-wide loading such as plate tectonic, overburden, topographic, and thermal stresses.

Because fracture formation and diagenesis are mutually dependent processes, cause–effect relationships between diagenesis and fracturing may be difficult to recognize based on the geologic record. Recognition of cause-effect relationships, however, would potentially allow prediction of fracture formation in the subsurface with likely applications in hydrocarbon and groundwater exploration and in toxic waste disposal.

This study combines petrographic and field observations with stable isotope analyses of cemented fractures or veins in the Miocene Monterey Formation in an attempt to correlate fracture formation and cementation with the burial diagenetic history of the sequence. The Monterey Formation, a hemipelagic sequence of siliceous mudstone, underwent a complex, but relatively well understood diagenetic alteration sequence during burial.

Based in part on stable isotopic data and largely on petrographic observations of apparent parageneses between vein and host-rock pore cement, it will be shown that the sequential order of vein cement reflects the diagenetic alteration of the host rock. In addition, fracture opening and cementation appear to coincide with specific stages of burial diagenesis suggesting that certain diagenetic alteration steps may favor fracture formation. The correlation between vein and pore cement is most obvious in host rock fragments which are abundant in all Monterey veins. Host rock fragments undergo diagenetic alteration, such as recrystallization and replacement, which becomes locked in at various stages through subsequent cementation of the interstitial fracture space. Gradual replacement and cementation of host rock, concurrent with vein cementation, can thus be observed in thin section. Host rock alteration is generally not restricted to the vicinity of fractures, however. A pore cement sequence similar to that seen in fractures is also observed in unfractured host rock.

The apparent correlation between host rock alteration and fracture opening and cementation will be tentatively explained by: 1.) presence of metastable phases in the host rock whose transformation to more stable phase is accelerated by fracturing and opening of the system to fluid flow; 2.) dehydration during phase transformation causing fluid flow and thus enhanced mass transfer from the rock matrix into the fracture system; 3.) mass transfer from the rock matrix into the fracture system, possibly enhanced by the generation of organic acids in the organic-rich host rock; and 4.) effects of dehydration reactions on fluid pressure increase and fracture opening.

Field observations and samples for petrography and

In: Eichhubl, P., ed., 1998, **Diagenesis, Deformation, and Fluid Flow in the Miocene Monterey Formation:** Pacific Section SEPM Special Publication, Book 83

isotopic analysis were collected from coastal exposures at Arroyo Burro County Beach in Santa Barbara (Figure 1), with additional observations from Ellwood and Rincon Beach. Description of veins focuses on the Arroyo Burro Beach section which contains the most complete sequence of distinguishable fracture generations with clear cross-cutting relationships.

Siliceous mudstone of the Monterey Formation contains abundant uncemented micro-faults and vein structures that, based on crosscutting relations, predate the cemented veins described in this study. The formation of these uncemented veins has been interpreted as penecontemporaneous to sediment deposition (Seilacher, 1969; Brothers and others, 1996; Grimm and Orange, 1997) and is not discussed further.

DIAGENESIS AND BURIAL HISTORY OF THE ARROYO BURRO BEACH SECTION

The Monterey Formation was deposited between about 19-6 Ma in a series of continental borderland basins in southern and central California (Pisciotto and Garrison, 1981; Barron, 1986; DePaolo and Finger, 1991; Miller, 1995). The sequence, rich in biogenic silica and organic matter, is composed of diatomite, porcelanite, chert, siliceous and phosphatic clay shale, and authigenic dolostone (Isaacs, 1981a, c). Subordinate are ash beds (Hornafius, 1994a) and phosphatic beds (Föllmi and Garrison, 1991). The formation, initially containing up to 34% organic matter (Isaacs and Petersen, 1987), is a source and fractured reservoir of hydrocarbons (Isaacs and Petersen, 1987; Ogle and others, 1989; MacKinnon, 1989).

Monterey rocks contain four principal rock-forming components to varying proportions (Isaacs, 1980, 1981a,c, 1983; Miller, 1995):

- silica phases, largely derived from diatoms and, in its least altered state, preserved as metastable opal-A;
- carbonate in form of calcite shell tests and as authigenic dolomite, the latter forming during early burial;
- clay, predominantly mixed-layer illite-smectite (Pollastro, 1990; Compton, 1991b);
- and organic matter, up to 34% in mudstone (Isaacs and Petersen, 1987).

These components undergo a series of diagenetic alterations during burial (Table 1):

- Opal-A is transformed to opal-CT and to quartz through two distinct steps of dissolution–reprecipitation (Murata and Nakata, 1974; Murata and Larson, 1975; Murata and Randall, 1975; Stein and Kirkpatrick, 1976; Pisciotto, 1981; Isaacs, 1981b, 1982; Behl and Garrison, 1994). Inferred temperatures of transformation in detrital-bearing siliceous mudstone are 45-50°C and 65-80°C for opal-A→opal-CT and opal-CT→quartz, respectively (Keller and Isaacs, 1985) (Table 1). The transformations occur at lower temperatures in pure silica rocks (Behl and Garrison, 1994; Behl, 1998).
- Early authigenic dolomite of lower cation ordering recrystallizes to dolomite of higher ordering (Compton, 1988; Malone and others, 1994).
- Illite-smectite clays increase systematically in illite component from about 10% to 80% over the temperature interval of 80-115°C (Compton, 1991b).
- Organic matter degrades through biotic and thermal processes to CO_2, CH_4, solid (bitumen) and liquid

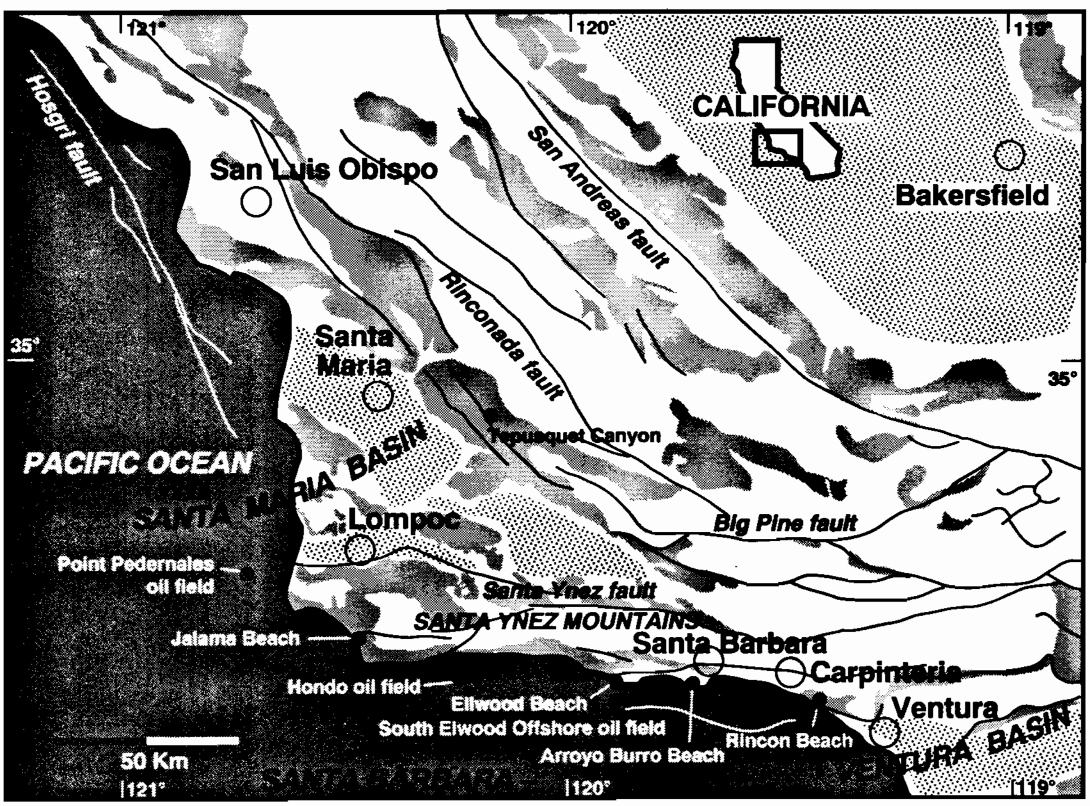

Figure 1: Map of locations mentioned in text. Shaded areas indicate exposures of Monterey Formation and age-equivalent units.

Fracture generation	Tectonic setting	Host rock diagenesis	Fracture cementation	Type of host rock	Fluid flow and mass transport	Tempera-ture [°C]	HC Fluid Inclusions
	- - -	bacterial methano-genesis, dolomite precipitation		organic-rich opal A diatomite	Mg^{2+} diffusion from sea water into sediment	<30?	
F1	basin subsidence	clathrate instability?	dolomicrite	siliceous dolostone	escape of methane and water	15-20?	no
		opal A → opal CT calcite recrystalli-zation		diatomite	silica diffusion on grain scale	45-50*	
F2		opal CT → quartz	quartz	siliceous dolostone	localized fluid flow on meter scale	40-50	no
F3	maximum burial	beginning cata-genesis of organic matter; recrystalliza-tion of dolomite	dolomite	(siliceous) dolostone, opal CT porcelanite	upward flow of isotopically heavy pore fluid	~55-65	no
	- - -	opal CT → quartz in deeper, unexposed parts of section		diatomite	silica diffusion on grain scale, locally advection	65-80*	
F4	folding/exhumation	catagenesis of organic matter, dissolution of calcite tests	calcite, bitumen; replacement of calcite by chalcedonic quartz	porcelanite and (siliceous) dolostone	episodic expulsion of pore fluid; beginning migration of hydrocarbons	~55-65	bitumen

Table 1: Diagenetic evolution at Arroyo Burro Beach and inferred timing of vein generations. Temperature estimates marked * after Keller and Isaacs, 1985.

hydrocarbons. Catagenesis begins at burial temperatures of about 60°C (Hunt, 1996; Isaacs and Petersen, 1987). The comparably low starting temperature of catagenesis has been explained by the high sulfur content of kerogen, facilitating thermal cracking (Petersen and Hickey, 1987).

The sequence at Arroyo Burro Beach consists of alternating, 5–20 cm thick beds of porcelanite and organic-rich, phosphatic mudstone. Dolostone forms 30–50 cm thick continuous beds, lenses, and concretions of up to 5 m in diameter. Porcelanite at Arroyo Burro Beach is in the opal-CT stage of silica diagenesis, whereas organic-rich phosphatic mudstone remained in the opal-A stage (Gross, 1993, 1995). Based on Keller and Isaacs' (1985) correlation between silica diagenetic grade and burial temperature, the section has experienced maximum burial temperatures of 45–50°C. Opal-CT in siliceous dolostone is partially replaced by quartz.

A ~0.5 m thick dolostone that is exposed repeatedly at Arroyo Burro Beach due to folding, is about 3 m above the Luisian/Mohnian stage boundary (Echols, 1994; Hornafius, 1994b) of about 13.8 Ma (Barron, 1986), This dolostone bed is host to many of the veins described in the following section. After slow burial during deposition of the Monterey Formation, burial accelerates during deposition of the Sisquoc and Pico Formations between 6 and 1 Ma (Figure 2, Table 2). The sequence reaches an estimated maximum burial of about 750 m shortly before its exhumation at about 1 Ma. Evidence for exhumation at 1 Ma is provided by the erosional base of the Santa Barbara Formation on Santa Barbara Mesa adjacent to Arroyo Burro Beach, unconformably overlying units of Miocene and Oligocene age (Olson, 1982; Dibblee, 1966, 1986a). At about 1 Ma, the beach section was exhumed to about 130 m below ground (Figure 2) based on the present elevation of the base of the Santa Barbara Formation on the Santa Barbara Mesa. The beach section underwent renewed subsidence of at least 150 m during deposition of the Santa Barbara Formation, corresponding to the erosional thickness of the Santa Barbara Formation on the Mesa (Dibblee, 1966) (Figure 2).

Folding of coastal section occurred as early as at the end of Monterey deposition and continues today (Feigl and others, 1993; Donnellan and others, 1993; Sylvester, 1995). Local angular unconformities between the Monterey and the overlying Sisquoc Formation and between the Sisquoc and the Plio/Pleistocene Pico Formation are observed about 5-20 miles west of Arroyo Burro Beach (More Mesa, Naples Beach) (Dibblee, 1966, 1986b, 1987). The Arroyo Burro Beach section is on the southern flank of the Mesa anticline (Olson, 1982) which may be considered part of the fold-structure forming the Santa Ynez Mountains. The Mesa anticline folded at about 1 Ma, prior to erosion of the sequence down to the Oligocene Sespe Formation and deposition of the Santa Barbara Formation. Outcrop-scale folds at Arroyo Burro Beach are coaxial and synkinematic to the Mesa anticline, based on the vergence of these outcrop scale folds with respect to the Mesa anticline. Outcrop-scale folding at Arroyo Burro Beach is therefore inferred to have occurred at around 1 Ma which is also considered the main stage of deformation in the Santa Ynez Mountains (Jackson and Yeats, 1982).

STRUCTURAL AND PETROGRAPHIC CHARACTERISTICS OF VEINS AT ARROYO BURRO BEACH

A sequence of four vein generations is observed at Arroyo Burro Beach (Table 3; see road log, this volume, for specific exposure locations). The earliest vein set, filled with micritic dolomite, is exclusively found in layers and lenses of authigenic dolostone. Dolomicrite veins are cut by quartz

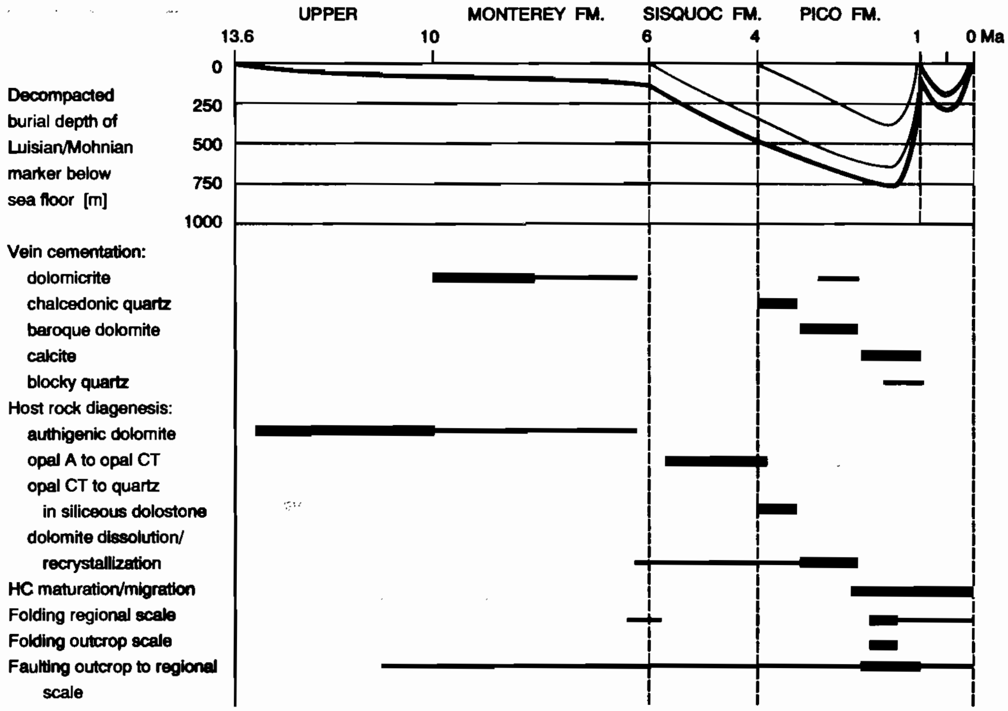

Figure 2: Burial history for the Arroyo Burro Beach section, shown with reference to the Luisian/Mohnian stage boundary which is about 3 m below a siliceous dolostone marker bed shown in Plate 1a. Maximum burial depth of about 750 m is reached shortly before uplift of the basin margin at about 1 Ma. Data and references underlying this reconstruction are listed in Table 2.

veins and breccias, occurring in siliceous dolostone and opal-CT porcelanite. Breccias and veins cemented by baroque dolomite are observed along low-angle reverse faults in dolostone, in part reactivating earlier quartz breccias. The most recent vein set is cemented by calcite, reactivates earlier vein generations or forms the first vein set in porcelanite and clay shale. Calcite veins are most extensively developed adjacent to, although not restricted to, mesoscale faults. Calcite veins are truncated by bitumen-cemented faults and brittle shear zones.

All four vein generations share the following characteristics: 1.) Veins are typically confined to beds of distinct composition, with exception of calcite veins adjacent to faults where these veins cut across the sequence. 2.) All vein generations typically contain abundant rock fragments. Quartz and baroque dolomite veins form breccia bodies rather than single veins. 3.) In quartz, baroque dolomite, and calcite veins, an initial 'event' of fracture opening and host rock brecciation allowed rotation and translation of rock fragments before subsequent cementation locked the fragments into place. Cementation after initial fracture opening and fragmentation began frequently with a geopetal layer of microcrystalline cement, lining the bottom of fracture space and the top of fragments. After partial or complete cementation of fracture and interstitial space, additional fracture opening episodes within each fracture generation may extend existing fractures or produce new ones, but not to the extent that rock fragments are free to rotate or translate. 4.) Quartz, baroque, and calcite veins also have in common rock fragments, contained in these veins, are stronger diagenetically altered than the host rock.

Dolomicrite veins (F1)

Dolomicrite veins are up to 10 cm thick, are preferentially perpendicular or parallel to bedding, with bedding-perpendicular veins striking on average E–W at Arroyo Burro Beach (Figure 3). Dolomicrite is typically laminated parallel to the fracture walls (Plate 1b), locally forming stratified sediment in fracture and breccia cavities (Plate 1a). Stratification is parallel to bedding of the surrounding host rock indicating fracture filling before tilting of the section by regional folding. Mutual crosscutting of vein cement laminae suggests that veins formed by the sequential infill of micrite. Dolomicrite veins include abundant fragments of host rock (Plate 1a) and of earlier vein cement (Plate 1b).

Dolomicrite is recrystallized to varying degrees. Least altered dolomicrite is organic-rich and brownish in thin section (Plate 1c), white in outcrop and may contain cryptocrystalline quartz (Plate 1d). Recrystallized dolomite forms euhedral rhombs about 10 mm in size, is clear in thin section, but dark gray in outcrop. Lamination becomes obliterated with increasing recrystallization. The elongate shape of isolated patches of unrecrystallized, organic-rich vein fill (Plate 1c) suggests that recrystallization and the removal of organic material is controlled by fluid percolation through the loosely cemented micritic vein fill.

Repeated events of fluid injection are apparent through cross-cutting of laminae within the same vein (Plate 1d), through mutual cross-cutting of different veins, and through erosional and aggradational bedforms of laminae (Plate 1b). Stratified (Plate 1a) and graded dolomicrite (Plate 1b) indicates deposition of detrital micrite out of suspension. Localized removal of organic material in the dolostone, apparently by fluid percolating through matrix pores in association with dolomicrite veins, suggests that the dolostone

Stratigraphic horizon	Age [Ma] at base	Reference	Thickness [m]	Reference	Water depth [m]	Reference	Porosity loss during compaction	Reference
upper Monterey Fm. (above Luisian/ Mohnian stage boundary ~ siliceous dolostone marker bed)	13.8 [1]	Echols, 1994; Barron, 1986	115 [1]	Arends & Blake, 1986; Hornafius, 1994c	1300	Arends & Blake, 1986	initial 90%, 60% after physical compaction, 30% after opal A to opal CT transition	Isaacs, 1981d, Compton 1991a
Sisquoc Fm.	6 [1]	Arends & Blake, 1986; Barron, 1986; Hornafius, 1994b	300 [2]	Jackson & Yeats, 1982	600	Arends & Blake, 1986	initial 90%, 60% after physical compaction	Isaacs, 1981d
Pico Fm.	4 [3]	Dumont, 1989	365 [2]	Jackson & Yeats, 1982; Olson, 1982	1000	Hsu et al., 1980	initial 40%, 15% after physical compaction	Wilson & McBride, 1988
Santa Barbara + Casitas Fm.	1 [4]	Huftile & Yeats, 1995	≥150 [5], ≤700 [6]	Dibblee, 1966	0	Dibblee, 1966		
End of deposition of Casitas Fm.	0.5 [7]	Jackson & Yeats, 1982; Levi & Yeats, 1993						

[1] at Naples Beach section
[2] in Summerland
[3] top of Siquoc in Santa Maria basin
[4] based on age of Bailey ash in Ventura area
[5] erosional thickness on Santa Barbara Mesa
[6] north of More Ranch fault
[7] based on correlation of Casitas Fm. with Saugus Fm. in Ventura basin

Table 2: Summary of data and references used for burial history reconstruction of the Santa Barbara coastal section (Figure 2).

Vein generation	Vein type	Subordinate vein fill	Country rock	Structure	Fabric	Inclusions
F1	Dolomicrite	Microcrystalline quartz, rock fragments	(Siliceous) dolostone	Bedding-confined, preferentially parallel and normal to bedding, breccias	Layered parallel to fracture walls, sedimentary geopetal layering	Finely dispersed organic matter
F2	Quartz	Microcrystalline quartz, rock fragments	(Dolomitic) porcelanite	Bedding-confined, random orientation, breccias	Bladed; microcrystalline quartz geopetal	Dolomite
F3	Baroque dolomite	Dolomicrite, rock fragements	(Siliceous) dolostone	Bedding-confined to irregular breccia bodies, random orientation	Bladed; dolomicrite geopetal	—
F4	Calcite	Calcmicrite, mega-quartz, calcedony, barite, rock fragments	Siliceous clay mudstone, porcelanite, (siliceous) dolostone	Adjacent to meso-scale faults, perpendicular to bedding, strike is fault-controlled, 'spalling'; extensive cementation along fault planes	Bladed; botryoids; inclusion-rich/-poor bands	Aqueous, bitumen

Table 3: Sequence and characteristics of vein generations observed at Arroyo Burro Beach.

was permeable for fluid percolation during dolomicrite vein formation.

Quartz veins (F2)

Quartz veins form stratabound breccia bodies in quartz-rich dolostone layers. Plate 1e shows the top half of a bedding-parallel breccia body, 3-5 cm thick, and completely cemented by quartz except for the uppermost vein cavity which is cemented by later dolomite and calcite.

The angular fragments of siliceous dolostone in quartz breccias are typically displaced and rotated without any evidence of transport beyond the hand sample scale (Plate 1e). Fracture filling columnar quartz has commonly radially sweeping (Plate 1g), patchy, sometimes feathery extinction suggesting recrystallization of chalcedony. Euhedral crystal terminations, seen through inclusion seams (Plate 1h) and, where preserved, as free crystal faces, indicate crystal growth into open, fluid filled fracture space. The outer margin of veins commonly consists of 10-30 mm wide, irregular zones of quartz cement which is rich in inclusions of finely dispersed dolomite and of organic matter (Plate 1h). These rims apparently formed by host rock displacement through vein filling quartz indicating that part of vein cementation occurs by outward growth through host rock replacement in addition to inward growth toward the vein center. Clear dolomite prisms within the replacement rims are evidence for dolomite recrystallization during partial replacement of host-rock dolomite by quartz.

Upward-facing fracture surfaces in quartz veins are frequently coated with smaller host rock fragments and with fine, partly recrystallized detritus of microflamboyant* quartz and dolomite. This detrital material, presumably dissolution residue after host rock replacement, is found deposited both directly on host rock surfaces as well as on earlier layers of quartz vein cement (Plate 1g). Similar to dolomicrite veins, stratified vein fill parallel to bedding of the country rock indicates vein cementation prior to regional folding.

Subparallel veins separate elongate host rock fragments which, as in Plate 1e, disaggregated after the main fragment had been detached from the host rock and rotated with respect to the sedimentary bedding. Fragmentation is therefore not a

Figure 3: Orientation of F1 (top) and F4 (bottom) veins at Arroyo Burro Beach. F1 and F4 veins differ in strike by 40-50° of clockwise rotation, consistent with paleomagnetic estimates of 5.8°/m.y. clockwise rotation of the Western Transverse Range since the Early Miocene. Present-day attitudes of F1 veins and of corresponding bedding surfaces (left) are rotated to their pre-folding position, obtained by rotating the associated bedding planes to horizontality (right). The pre-folding origin of F1 veins is indicated by stratification of fracture-filling sediment being parallel to bedding. Normal faults which accommodate the extensional strain of F4 calcite veins in under- and overlying mudstone beds are coaxial to NE–SW striking F4 veins.

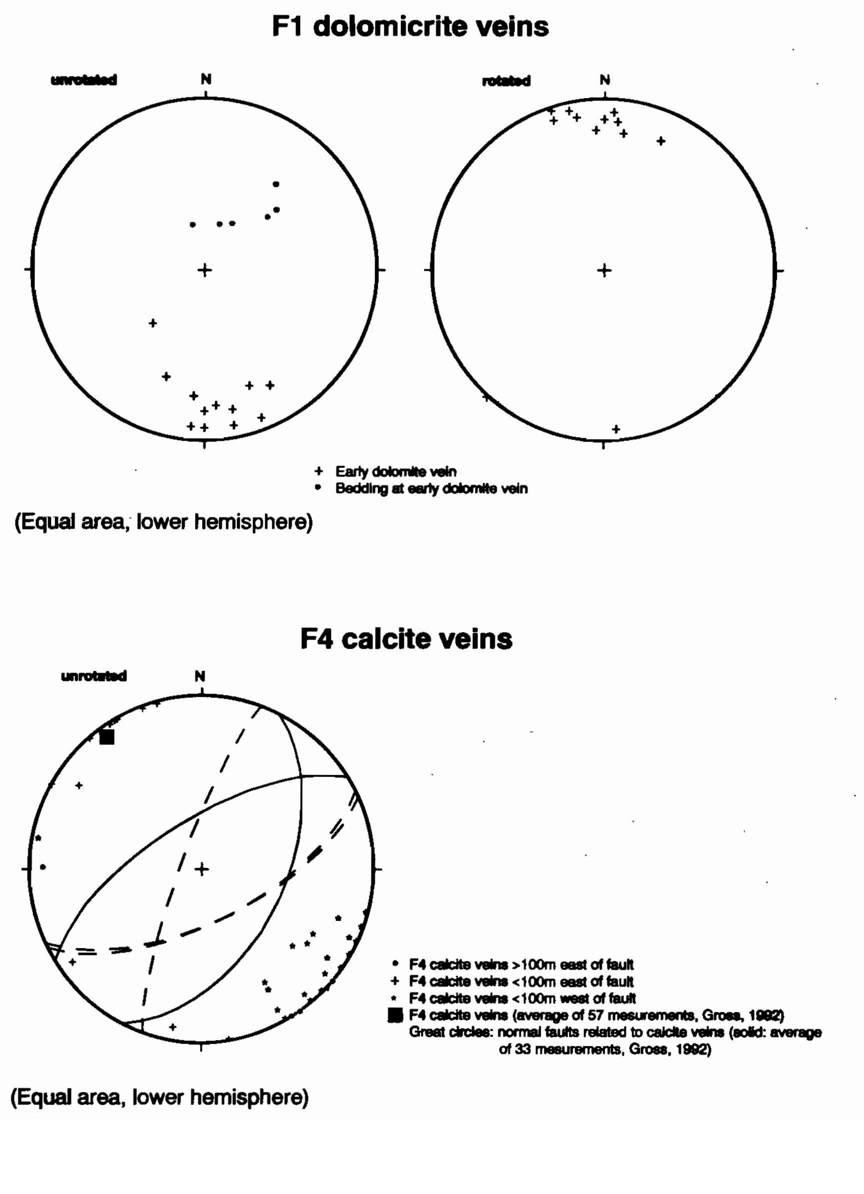

single event but rather continues after initial brecciation and cementation. This continued vein formation does not isolate host rock fragments to an extent which allows further rotation of fragments.

Breccia components of siliceous dolostone show different amounts of dissolution and replacement of dolomite by quartz (Plate 1f). Unaltered fragments of siliceous dolostone in the sample depicted in Plate 1f are composed predominantly of dolomite with an estimated silica cement volume of less than 10%, whereas altered fragments are almost completely replaced by quartz. Dolomite is clearly dissolved and removed in solution while silica is added into the fracture system on a local scale. Dolomite is dissolved in part by surface corrosion of fragments and in part by dissolution of matrix dolomite within fragments, in both cases being replaced by quartz.

Cementation of quartz veins appears to be synchronous to opal-CT dissolution and quartz precipitation in the siliceous host rock. Plate 2a and b show quartz cemented F2 fractures from a somewhat less dolomitic part of the same siliceous dolostone bed at Arroyo Burro Beach as shown in the previous examples. Both opal-CT and microflamboyant quartz are present in the host rock, quartz being precipitated preferentially in pores (Plate g). Apparently, the transformation of opal-CT into quartz in the host rock of this layer did not go to completion.

Because quartz cemented fractures are only seen in samples that also contain at least some diagenetic quartz in the matrix, it is suggested that quartz vein cementation in Plate 2a was synchronous to opal-CT dissolution and quartz precipitation in the matrix of the host rock.

Silica transformation is accompanied by some recrystallization of dolomite, seen as euhedral crystals of clear dolomite precipitating both in the host rock (Plate g) and in fractures (Plate 1h) together with quartz. Dolomite dissolution and recrystallization becomes more pervasive during the subsequent stage of baroque dolomite vein formation.

Baroque dolomite veins (F3)

The third generation of veins at Arroyo Burro Beach, cemented by baroque dolomite and minor amounts of dolomicrite, forms breccias along low-angle thrust faults or reactivated earlier quartz cemented veins. Dolomite cemented veins are found exclusively in host rock which contains dolomite, e.g. dolostone or dolomitic porcelanite.

Dolomite crystals in F3 veins at Arroyo Burro Beach are typically bladed, 30-100 mm in size, with curved crystal faces and sweeping extinction in cross-polarized light (Plate2d), characteristic of baroque dolomite. The warped crystal lattice of baroque dolomite is caused by the incorporation of excess Ca^{2+} in Mg sites and is considered characteristic of burial temperatures between 60 and 150°C (Radke and Mathis, 1980). Crystal terminations are idiomorphic indicating growth into open space. The contact to host rock or host rock fragments is usually diffuse through corrosion and recrystallization of host rock dolomite along fracture surfaces. Tops of fragments are commonly covered with a few micrometer thick layer of dolomicrite (Plate2c, Plate2e).

*cryptocrystalline: <1mm, microcrystalline (straight extinction) and microflamboyant (undulatory extinction): 1-20mm, megacrystalline: >20mm (Behl and Garrison, 1994)

Dolomicrite also fills residual fracture space after precipitation of columnar dolomite. This dolomicrite may be stratified parallel to bedding of the host rock (Plate 2h).

Analogous to earlier quartz veins, breccia fragments in baroque dolomite veins are variably altered and replaced, in this case by dolomite (Plate2e and f). Host dolomite, typically with a crystal size of less than 30 mm and rich in inclusions of organic matter, recrystallizes to a mosaic of equant, inclusion-free crystals of baroque dolomite exceeding 30 mm (Plate 3a). Opal-CT, originally contained in host rock fragments, goes apparently in solution during dolomite replacement, because quartz or other silica phases are not coprecipitated with dolomite (Plate 2e and f, Plate 3b). Quartz is found in residual interstitial space after F4 calcite vein fill or, where calcite is not precipitated, after F3 baroque dolomite (Plate 3b).

Dissolution and re-precipitation of dolomite matrix cement is enhanced but not restricted to the vicinity of veins. Siliceous dolostone at Arroyo Burro Beach consists of interlocked rhombs of dolomite with, from lamina to lamina, varying amounts of organic matter and pore-filling microflamboyant quartz. Organic-rich laminae are quartz free, composed of anhedral, <50 mm dolomite crystals with organic matter being partly dispersed as solid inclusions, partly concentrated along grain boundaries. Organic-poor laminae contain up to 30% quartz which is typically clustered in nests of up to 1 mm in size. Dolomite crystals in organic-poor laminae exceed 50 mm in size, are frequently euhedral and inclusion-free or with inclusion-rich cores and clear rims (Plate 3c).

Calcite veins (F4)

Structural context

The youngest vein generation is most extensively developed adjacent to mesoscale faults but is also observed away from faults as bedding-confined veins, in part reactivating earlier vein sets (Plate 1a, Plate 3d). These veins are cemented by calcite and solid hydrocarbon or bitumen at Arroyo Burro Beach. Veins with similar structural characteristics, but cemented by dolomite, are observed at Jalama Beach (Figure 1) (see road log, this volume, stop 2).

Formation of bedding-confined veins (Plate 3e) is apparently controlled by host rock composition. In under- and overlying beds of clay shale, the extensional strain of these veins is accommodated by conjugate sets of normal faults. The partitioning of bedding-parallel extension into veins and normal faults, controlled by host rock composition, has been described by Gross and Engelder (1995), Gross (1995), and Sibson (1996) from Arroyo Burro Beach. Bedding-confined calcite veins are found preferentially next to normal faults of 1-10 m scale, transecting and offsetting the porcelanite layer by up to 15 cm (Figure 6). These faults extend from the porcelanite layers up to 5 m into the over- and underlying beds of clay shale.

Massive amounts of calcite vein cement are observed adjacent to two mesoscale faults, exposed in the beach cliffs about 600 m east of the Arroyo Burro County Park and 110 m apart (see road log, this volume, stop 1). The fault zones are extensively cemented by calcite, arranged in radiating aggregates of bladed crystals forming 10-30 cm thick botryoids. Bitumen fills typically any residual fracture space after calcite. Along the fault surfaces, calcite vein cement is fragmented and cemented by bitumen.

The host rock sequence of porcelanite and clay shale within 5-10 m to both sides of the faults is densely transected by calcite veins. Although veins cut across the porcelanite and clay shale sequence, vein thickness is controlled by host rock composition. Vein apertures are widest in siliceous dolostone and porcelanite. Veins splay and thin out when entering under- and overlying mudstone beds. Veins resume their orientation and thickness where they transect the next porcelanite bed (Plate 3f). Well developed veins extend across the sequence for >10 m perpendicular to bedding. These continuous veins apparently form through linkage of fractures which initiate independently in individual porcelanite and dolostone beds and connect across mudstone beds in between.

Calcite-cemented F4 veins, similar to earlier quartz and baroque dolomite veins, are characterized by abundant breccia fragments, either floating as isolated pieces in a matrix of calcite cement or forming breccia dikes with calcite and bitumen filling the interstitial space (Plate 3f). Fragmentation of the host rock adjacent to veins is apparently the result of fracture clustering (Plate 3g), i. e. the increase in vein density adjacent to larger veins (Figures 4 and 5) or faults (Figures 6 and 7). Sets of closely spaced, subparallel fractures, in conjunction with orthogonal fractures, cause the host rock to become fragmented and eventually completely isolated from the fracture wall. Increased vein density does not appear to be caused by differential slip along veins although brecciated veins may be reactivated in shear. Clustering of veins is apparent from the vein frequency distribution (Figures 8 and 9): Instead of being centered around some mean spacing value with a normally distributed deviation, the frequency distribution of Monterey veins is heavily skewed toward narrow vein spacing. With a higher number of narrow than of wide spacings, narrowly spaced veins are necessarily grouped together, forming concentrations or clusters. The minimum fracture spacing does not approach the minimum resolution of the fracture traverses of 5 mm for vein spacing but rather saturates at a mode of about 2 cm for porcelanite (Figure 8) and 10-15 cm for dolostone (Figure 9). The difference in spacing may be controlled by host rock composition and/or by bedding thickness. The measured dolostone beds are ~0.5-1 m thick, porcelanite typically 5-20 cm. The frequency distribution of vein spacing in porcelanite host rock is similar for veins next to the mesoscale faults and for veins adjacent to faults in the 1-10 m scale shown in (Figure 6).

Stratified vein fill that is horizontal and discordant to sedimentary bedding of the host rock suggests that F4 veins postdate folding at about 1 Ma.

Away from any local disturbance through mesoscale faults, calcite veins strike on average NE–SW at Arroyo Burro Beach (Figure 3), at about 45-50° with respect to F1 dolomicrite veins. Based on the paleomagnetic data by Hornafius (1985) and Hornafius and others (1986), the western Transverse Ranges have undergone about 100° clockwise rotation in the last 17 m.y. or about 70° in the last 12 m.y. (Luyendyk, 1991). The difference in orientation between F1 and F4 veins at Arroyo Burro Beach may reflect this rotation. Luyendyk's (1991) linear regression to the data of Hornafius and others (1986) of 5.8°/m.y. gives an age difference of about 6.9-8.6 m.y. between F1 and F4 veins. Assuming that F4 veins formed at about 1 Ma, F1 veins would have formed at about 7.9-9.6 Ma. Assuming a constant sedimentation rate of 19 m/m.y. between 12 and 6 Ma, F1 veins would have formed at a predicted burial depth of 83-116 m. This depth range is consistent with inferred burial temperatures based on the stable isotopic composition given in the next section.

Solid hydrocarbon or bitumen is common as fracture fill in the Monterey Formation. Bitumen may follow earlier cements, usually calcite, or may be the only fracture fill. Bitumen-cemented, brecciated brittle shear zones offset calcite veins at Arroyo Burro Beach (see road log, this volume, stop 1). In case of reactivated earlier breccias, bitumen is the last vein filling phase, which may be taken as indication that bitumen filling of fractures postdates all earlier phases of fracture cementation. Alternatively, bitumen may just inhibit further cementation in which case the observation that bitumen is the last phase would have no implication on the timing of bitumen filling within the overall sequence of vein cements. Bitumen is found as primary inclusions in F4 calcite veins.

Vein morphology, vein composition, and host rock alteration

Similar to quartz and baroque dolomite veins, calcite veins are characterized by initial fracture opening and fragmentation, rotation and translation of fragments, deposition of stratified micrite, complete cementation, and subsequent widening of cemented fractures (Plate 3d, Plate 3h).

In calcite veins, corrosion, dissolution, and replacement of host rock fragments are less pervasive than in F2 and F3 veins. Fragments may become cemented without any visible dissolution or corrosion as in Plate 4a. In some cases, corrosion is very localized (Plate 4b): Of two adjacent fragments of similar rock type, one is locally corroded whereas the other one preserved its primary angularity. This selective dissolution may be interpreted either as evidence for protective cement coatings around fragments, similar to ones observed by Behl and Smith (1992) in chert breccias. Alternatively, locally different wetting characteristics of water versus oil may have controlled host rock corrosion. Other fragments, predominantly those rich in organic matter, disintegrate into smaller pieces (Plate 4c) rather than being entirely dissolved. Fragment corrosion predates cementation as illustrated in Plate 3h where micrite blankets the top of a corroded fragment.

Because fracture walls and fragments are less corroded than in earlier vein generations, details of continued fracture extension after initial cementation can be observed. Thin seams of host rock inclusions parallel to fracture walls (Plate 4d), outlining the shape of the host rock fragments, are clear evidence for crack-seal fracturing. Apparently, after initial brecciation and subsequent cementation, the rate of cementation kept up with the rate of fracture extension. Most veins are cemented by crystal growth into open space, however, recognized by euhedral crystal terminations as in Plate 4e. Although continued fracture opening during cementation cannot be demonstrated in these cases, it is

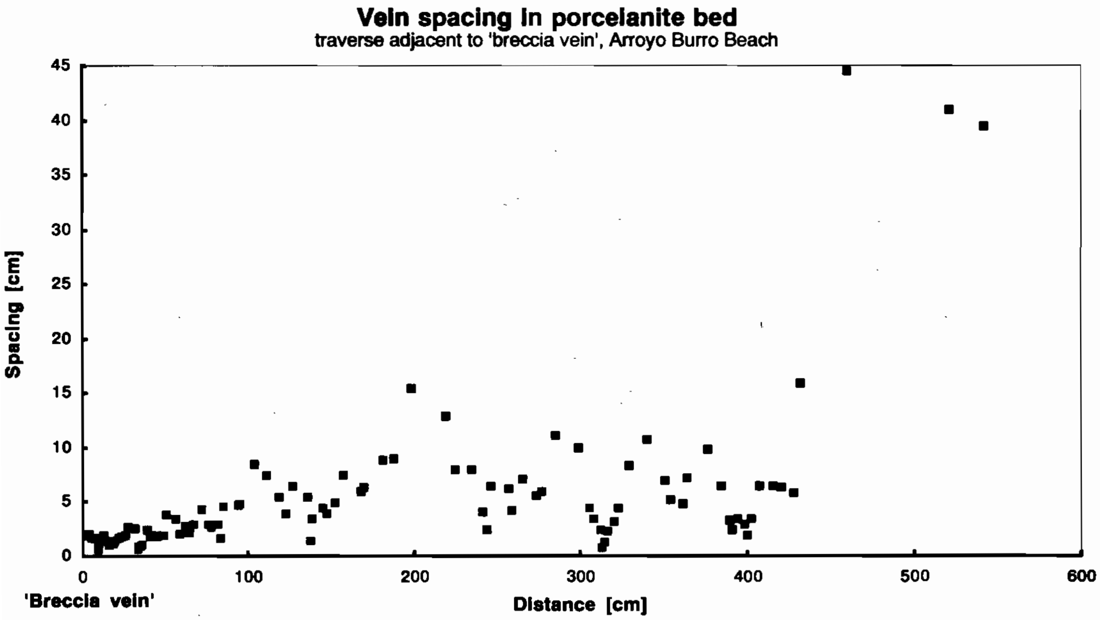

Figure 4: Spacing of layer-confined veins in a 3 cm thick porcelanite bed increases with increasing distance from a major breccia-filled through-going vein at Arroyo Burro Beach, 45 m east of the eastern fault.

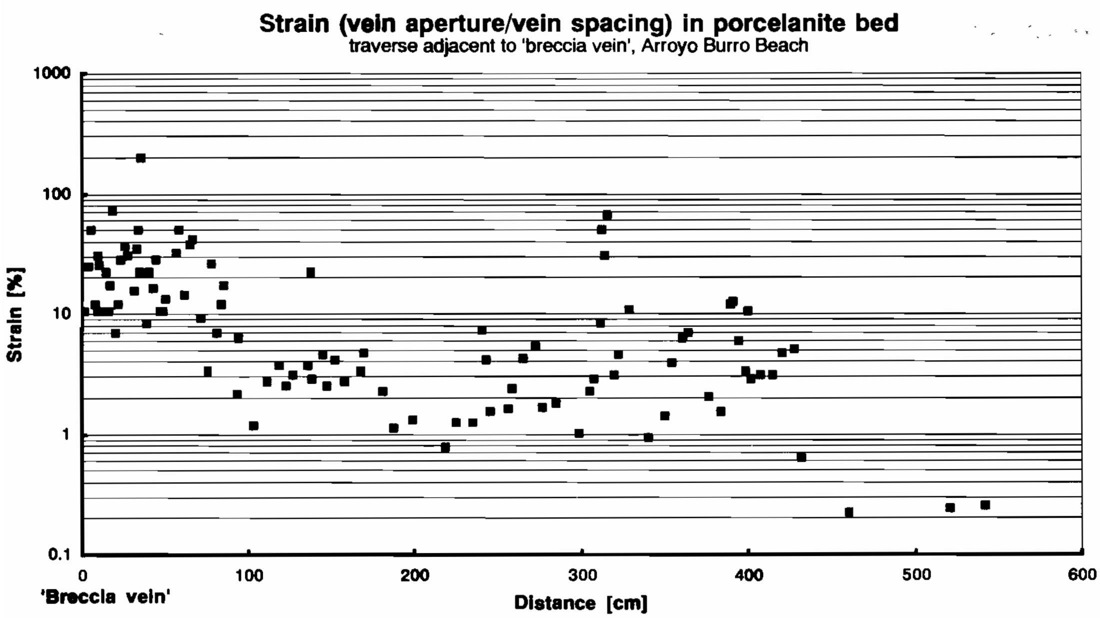

Figure 5: The same fracture traverse of Figure 4 expressed as fracture strain (vein aperture/ vein spacing), showing a steady decrease in strain with increasing distance from the through going vein.

apparent that the permeability of these fracture systems depends on a balance between the rate of fracture opening and the rate of fracture cementation. Even cementation in the crack-seal vein of Plate 4d was eventually outpaced by fracture opening, evident by bitumen filling the last opening increment (lower left in Plate 4d, replaced by clear epoxy during thin section preparation).

Rotation and transport of fragments indicates that initial fragmentation and cementation occurred in sequence. Rotation and transport requires that fragments were completely detached from the wall rock prior to cementation of the fracture space. This may imply that fragmentation occurred while fluid conditions did not allow precipitation at the time of fragmentation but changed in favor of cementation at some later time. Alternatively, fragmentation and fragment transport may have occurred relatively fast compared to the rate of calcite precipitation even though the fluid was oversaturated with respect to calcite. Initial fragmentation preceding cementation is also demonstrated through micritic calcite, forming a thin layer on top of breccia fragments. Detrital micrite apparently settled through the fluid filled breccia cavities prior to cementation. The observation of micrite sitting on already corroded fragment surfaces (Plate 3h) argues for variations in fluid saturation conditions rather than kinetic arguments to explain the temporal separation of brecciation and cementation.

Evidence of cementation into open fracture space is particularly abundant along the two fault zones at Arroyo Burro Beach which are cemented by radiating aggregates of bladed calcite crystals forming 10-30 cm thick botryoids.

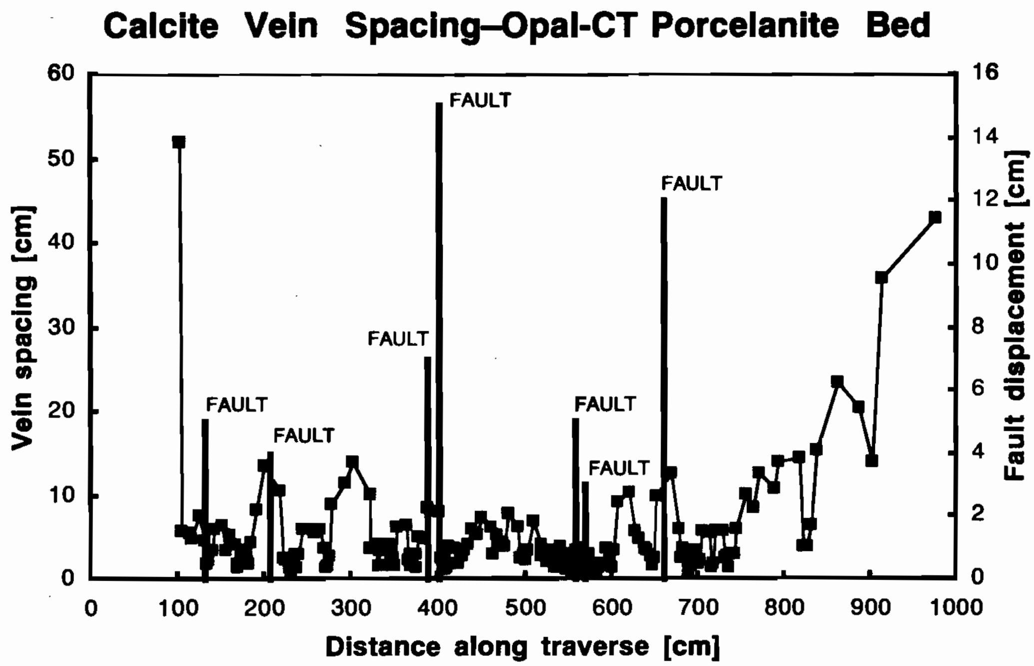

Figure 6: Vein spacing of calcite veins confined to ~10 cm thick porcelanite layer at Jalama Beach. Veins are found adjacent to normal faults, offsetting the porcelanite layer by up to 15 cm (right-hand scale of plot). A section of the measured traverse is shown in Plate 3e.

Calcite contains alternating bands of inclusion-rich and inclusion-poor layers (Plate 4f), with single-phase aqueous and bitumen inclusions. Based on fluid inclusion microthermometry of similar vein cement at Jalama Beach where both single- and two-phase aqueous fluid inclusions occur (Eichhubl, 1997), single-phase aqueous inclusions indicate fluid temperatures of less than ~65°C. Bitumen inclusions indicate vein cementation during hydrocarbon maturation. Liquid hydrocarbons are rare as primary fluid inclusions which suggests that the Arroyo Burro section has not fully entered the oil window. Bitumen as the final cement is particularly abundant within the eastern fault zone.

When cementation could not keep up with fracture opening, fractures were potentially effective conduits for fluid flow. Evidence for fluid flow after initial brecciation is provided by sedimentary lamination and fragment transport in veins (Eichhubl, 1997). Alternating laminae of micrite and bladed calcite, micrite preferentially filling the V's between apices of idiomorphic crystal terminations (Plate 4g), suggest cyclic changing flow conditions. Micrite fills the topography of idiomorphic calcite crystal terminations which suggests deposition of micrite as detrital material (Plate 4e) rather than precipitation *in situ*.

Cathodoluminescence reveals two cycles of banding in inclusion-poor calcite, a coarser cycle of gradual decrease in luminosity on a 1000 to 100 µm scale, and oscillating luminescence bands superposed on the first cycle on a 1 µm scale (Plate 4h). All types of banding outline the shape of

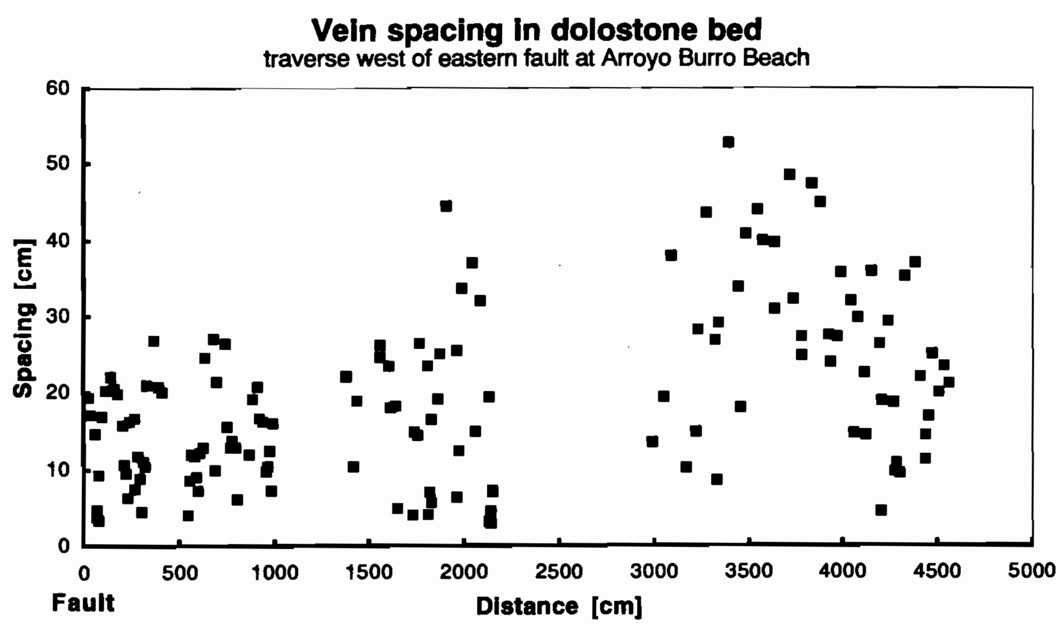

Figure 7: Vein density decreases with increasing distance from the eastern fault at Arroyo Burro Beach. While the maximum spacing increases, the minimum spacing remains about the same, indicating that veins are clustered on a meter to centimeter scale, in addition to the outcrop scale. Traverse follows a 30-50 cm thick dolostone layer.

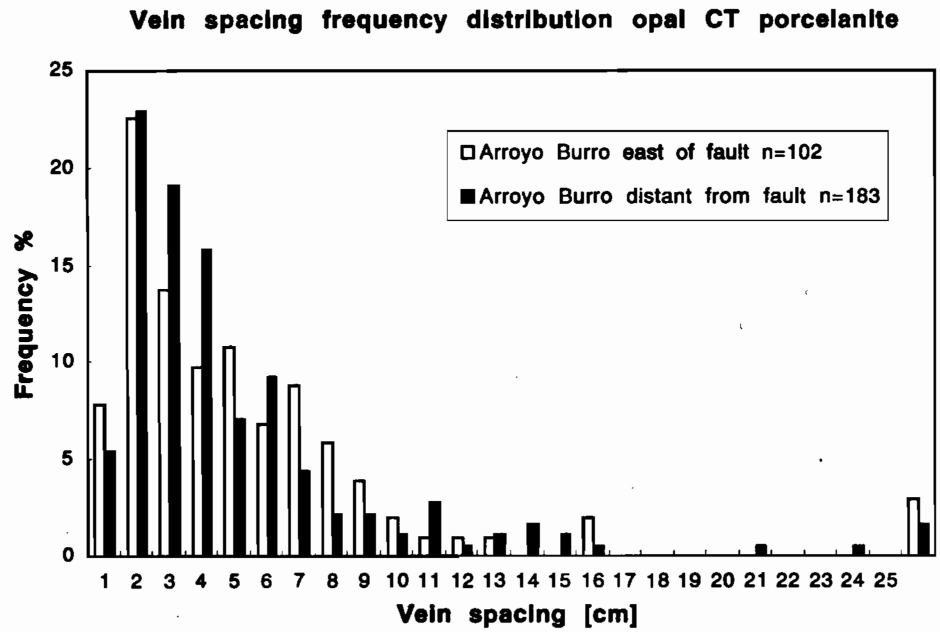

Figure 8: Vein spacing frequency distribution in opal CT porcelanite from Arroyo Burro Beach. The first data set corresponds to the vein spacing traverse in Figure 4, 45 m east of the eastern fault at Arroyo Burro Beach. Bed thickness is about 3 cm. The second data set is from a cluster of veins around decimeter to meter scale normal faults about 400 m east of the eastern fault (Plate 3e). Bed thickness is about 10 cm. Despite differences in bed thickness and differences in scale of the fault-vein system, vein spacing at both traverses saturates at 2 cm. The distribution is similarly skewed as the distribution for dolostone although with a lower mode.

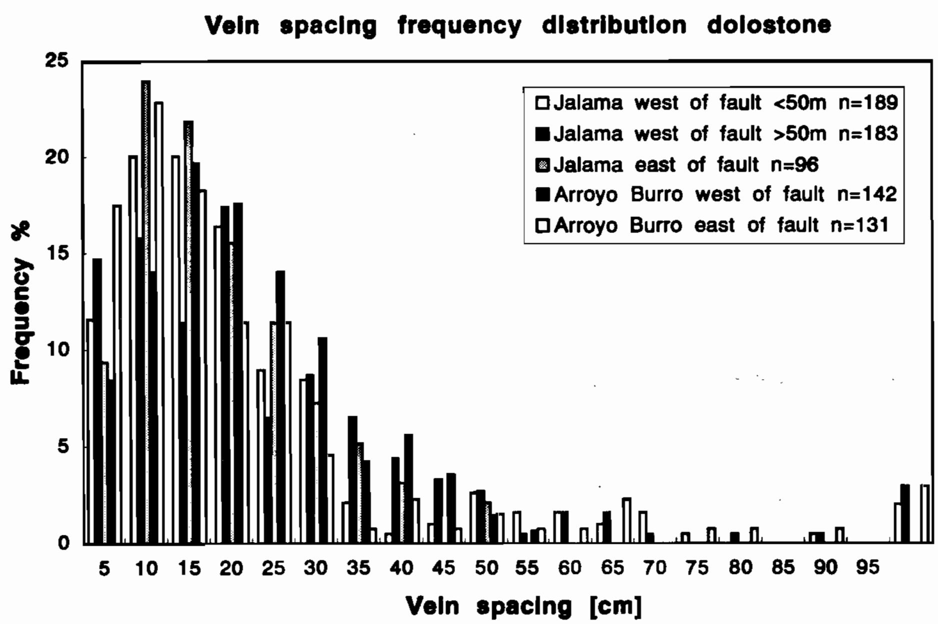

Figure 9: Frequency distribution for carbonate veins in dolostone layers adjacent to faults at Arroyo Burro and Jalama Beach. The frequency distribution is skewed towards narrow spacing implying that veins are clustered rather than equally spaced as common for joints. Fracture spacing appears to saturate at about 10 cm. The resolution of the traverse is 5 mm for spacing and 1 mm for vein thickness. The mode value is apparently independent of distance from the fault at Jalama Beach and is about the same for both locations, therefore also independent of vein cement composition (dolomite at Jalama Beach, calcite at Arroyo Burro Beach) and bed thickness. Bed thickness is about 50 cm at Arroyo Burro Beach and 10 cm at Jalama Beach.

euhedral crystal terminations, indicative of cement growth into open space.

Calcite in F4 veins hosted in siliceous dolostone may be followed by late stage quartz. Calcite may also be replaced by chalcedonic or megaquartz containing inclusions of dolomite (Plate 4c).

THE STABLE ISOTOPIC COMPOSITION OF VEIN CEMENT AT ARROYO BURRO BEACH

The carbon and oxygen isotopic composition of carbonate fracture fill and of host dolostone at Arroyo Burro Beach is plotted in Figure 10 and listed in Table 4. Vein cement for these analyses was sampled with a micro-drill and stable isotopic analyses of carbonate and silicate samples were performed by Kurt Ferguson at Southern Methodist University, Dallas. All $\delta^{18}O$ values for dolomite were corrected for a reaction temperature of 50°C following Rosenbaum and Sheppard (1986). Mixed quartz–carbonate samples of vein cement and host rock were analyzed through selective dissolution of carbonate before silicate analysis. Repeats of every fifth analysis indicate that reported $\delta^{18}O$ and $d^{13}C$ values are reproducible within ±0.2‰. $\delta^{18}O$ and $\delta^{13}C$ values of carbonate are reported with respect to the PDB standard, $\delta^{18}O$ values of silicate and water with respect to SMOW.

The stable isotopic composition of formation water was

Figure 10: Stable isotopic composition of vein and host rock carbonate at Arroyo Burro Beach, with additional data from Ellwood and Rincon Beach, and data from Winter and Knauth (1992) for Carpinteria Beach. The initial trend towards isotopically heavy carbon and near-zero oxygen values, changing to increasingly lighter carbon and oxygen values reflects organic matter degradation and temperature increase during burial. E: Ellwood Beach, R: Rincon Beach, C: Carpinteria Beach; numbers designate relative sequence of cementation. Data are listed in Table 4.

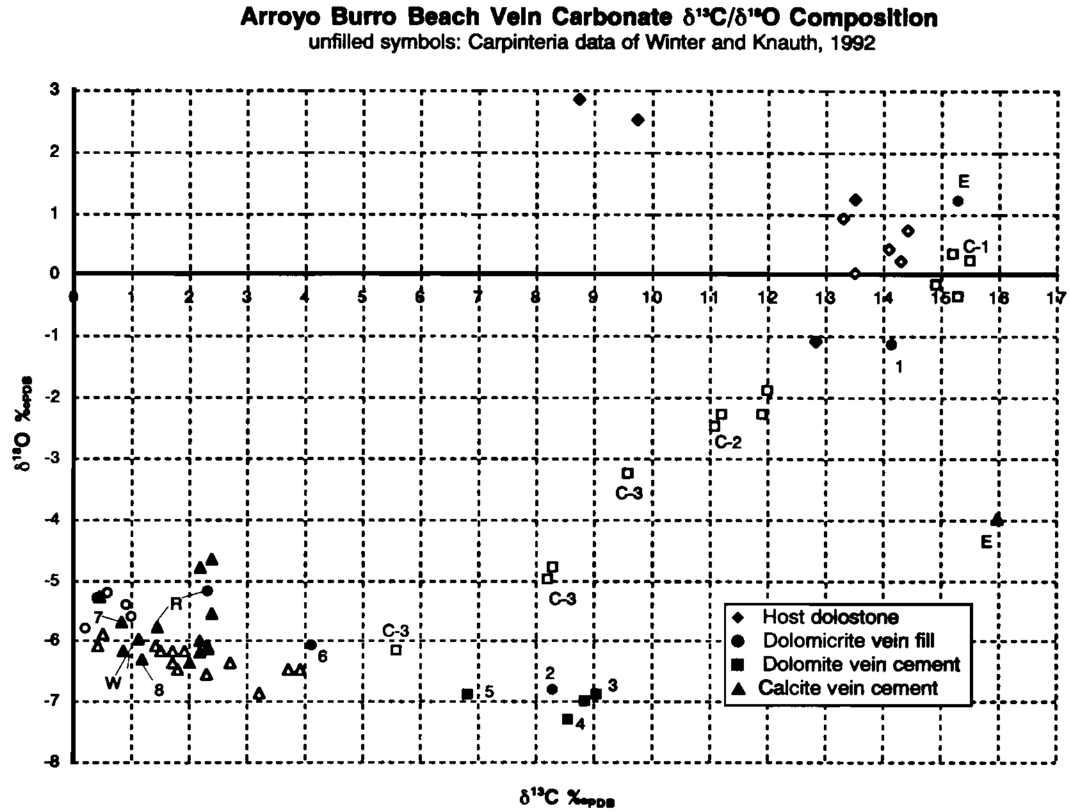

also analyzed from producing wells in the Elwood and Hondo offshore oil fields (Table 5). The $\delta^{18}O_{SMOW}$ composition of present-day formation water, plotted versus deuterium in Figure 11, ranges between +2 and +6‰.

Dolomicrite veins (F1)

The least recrystallized dolomicrite vein fill at Ellwood Beach has a stable isotopic composition of $\delta^{18}O_{PDB}$ +1.2‰ and $\delta^{13}C_{PDB}$ +15.3‰ (Figure 10). The light oxygen and heavy carbon composition suggests an early origin of these veins in the zone of microbial methanogenesis (Winter and Knauth, 1992). Similar, but slightly coarser and thus presumably recrystallized dolomicrite at Arroyo Burro Beach has a $\delta^{18}O_{PDB}$ and $\delta^{13}C_{PDB}$ composition of -1.1‰ and +14.1‰, respectively. Vein cement $\delta^{18}O_{PDB}$ is somewhat lighter and $\delta^{13}C_{PDB}$ somewhat heavier compared to the isotopic composition of the host dolostone. The $\delta^{18}O_{PDB}$ composition of the dolostone host rock is a heavy as +3‰, $\delta^{13}C_{PDB}$ as light as +13.5‰. Similar values have been reported by Winter and Knauth (1992) for Carpinteria Beach, which are also shown in Figure 10.

Assuming the pore fluid $\delta^{18}O_{SMOW}$ composition during dolomicrite vein cementation is similar to Late Miocene sea water of -0.7‰ (Feary and others, 1991), and using the dolomite–water fractionation factor by Matthews and Katz (1977), temperatures of precipitation of 20°C at Ellwood and 31°C at Arroyo Burro Beach are obtained. The early low-temperature origin of these veins is consistent with bedding-parallel stratification of micritic vein fill (Plate 1a), evidence for vein formation prior to folding which tilted both bedding and stratified fracture fill by an average of 50-60° at Arroyo Burro Beach.

The sedimentary structures in the dolomicrite are evidence for transport of micrite as detritus. This leaves three alternatives as to its origin: Dolomicrite may represent residue after partial host rock dissolution, or it may have formed by precipitation either before or during transport. As a third alternative, in between the two other extremes, precipitation may have occurred on seeds provided by incomplete host rock dissolution. If the dolomicrite contains a significant host rock component, then the isotopic composition would bear little as to the origin and timing of F1 veins. Because the carbon isotopic composition of dolomicrite vein fill is typically heavier or more 'methanogenic' than the host dolostone, dolomicrite contains at least a large component of carbon which is not derived from host rock dissolution but rather directly from microbial metabolism. Dolomicrite is thus mostly a precipitate.

Dolomicrite veins cut and therefore postdate authigenic formation of dolomicrite beds. The heavy $\delta^{13}C$ composition, on the other hand, indicates they still formed during late stages of microbial methanogenesis. The formation of F1 dolomicrite veins is plotted therefore after authigenic dolostone formation on the burial curve in Figure 2. Eichhubl (1997) discussed the possibility that dolomicrite veins reflect episodic escape of methane after thawing of solid methane clathrate.

sample #	absolute/ relative sequence	subsample #	composition	$\delta^{13}C$	$\delta^{18}O$ PDB	$\delta^{18}O$ SMOW
Arroyo Burro Beach						
calcite vein in porcellanite (360 m W stairs, wavecut platform)						
03/14/95-2	F4	B23	calcite vein	0.45	-5.26	25.44
breccia vein in siliceous dolostone marker bed (260 m W stairs, below pipe)						
04/25/94-5	0/a	A6	disseminated dolomite	12.81	-1.07	29.76
same	0/b	A6	qtz cement			28.20
same	F2/a	A7	qtz vein			24.33
same	F2/b	A1	qtz vein			20.92
same	same	A14	same			20.91
same	F3/a	A3	geopetal dol micrite	8.30	-6.80	23.85
same	F3/b-d	A4	baroque dol vein	8.57	-7.30	23.33
same	F3/b	A8	baroque dol vein	9.07	-6.88	23.77
same	F3/c	A9	baroque dol vein	8.84	-6.99	23.65
same	F3/d	A10	baroque dol vein	6.81	-6.87	23.78
same	F3/e	A5	dolomicrite	4.13	-6.07	24.60
same	F4/a	A2	calcite vein	0.84	-6.15	24.52
same	same	A15	same	1.11	-5.97	24.71
same	F4/b	A2	qtz replacement			27.47
same	same	A15	same			24.17
micrite vein in siliceous dolostone (350 m W stairs, wavecut platform, plate 1a)						
02/24/95-3BN	0	C19	host dol lamina	13.50	1.23	32.13
02/24/95-3B2	F1	C15	stratified cc? micrite	14.21	-0.45	30.40
same	F1	same	stratified dol micrite	14.19	-1.19	29.63
same	same	repeat	same	14.10	-1.08	29.75
02/24/95-3BB	F2	C18	quartz vein			26.10
same	F4/a	C16	coarse xx vein cc	0.83	-5.68	25.00
same	F4/b	C17	cc micrite vein	1.17	-6.30	24.37
fault 600m E county beach						
03/14/95-3	F4/a	B4	banded calcite	2.38	-5.53	25.16
same	F4/b	B5	same	2.39	-4.64	26.08
same	F4/c	B6	same	2.18	-4.80	25.91
same	same	repeat	same	2.18	-4.78	25.93
03/13/95-2	F4/d?	B7	calcite micrite	2.19	-6.10	24.57
breccia vein 20 m E fault						
03/13/95-6	F4/a	B1	interstitial calcite	2.32	-6.11	24.56
same	F4/b	B2	calcite vein fill	2.31	-6.16	24.51
same	same	repeat	same	2.30	-6.11	24.56
same	F4/c	B3	same	2.17	-6.19	24.48
siliceous dolostone marker bed (55 m E fault)						
06/03/96-1		C20	siliceous dolostone	8.73	2.87	33.82
siliceous dolostone marker bed (13 m E fault)						
06/03/96-2		C21	same	9.74	2.53	33.47
Rincon Beach						
dolostone bed						
02/06/95-3	F4?/a	C23	high Fe cc vein fill	1.43	-5.78	24.90
same	F4?/b	C22	high Fe dol micr vein	2.31	-5.17	25.53
Ellwood Beach						
dolostone bed						
05/02/95-2	F1	B25	dolomite micrite vein	15.29	1.20	32.10
05/02/95-1	F4	B24	calcite vein fill	15.98	-4.02	26.72
same	same	repeat	same	15.95	-3.95	26.79

qtz: quartz, cc: calcite, dol: dolomite, xx: crystalline, micr: micritic

Calcite fractionation after Friedman & O'Neil, 1977
Dolomite fractionation after Matthews & Katz, 1977
Quartz fractionation after Matsuhisa et al., 1979

absolute sequence attempts regional correlation for all fracture generations (Table 1)
relative sequence is based on cross-cutting relations for a single outcrop

Table 4: Stable isotopic composition of vein and host rock carbonate and silicate at Arroyo Burro Beach, Ellwood Beach, and Rincon Beach.

Quartz veins (F2)

The $\delta^{18}O_{SMOW}$ composition of chalcedonic quartz in two F2 veins from Arroyo Burro Beach is 26‰ for one of the veins, and 24‰ and 21‰ in the second vein, the last two values referring to earlier and later cement of the same vein. Quartz cement in the siliceous host dolostone has a $\delta^{18}O_{SMOW}$ composition of 28‰. Assuming a Miocene sea water $\delta^{18}O_{SMOW}$ composition of -0.7‰, the last value gives a precipitation temperature of 51°C. This is well below the temperature of the opal-CT to quartz transition in clay-containing porcelanite at 65-80°C (Keller and Isaacs, 1985) but in the range of quartz precipitation for 'pure' opal-CT protoliths which is 36-76°C, according to Behl and Garrison (1994) and Behl (1998).

Assuming the same fluid composition of -0.7‰$_{SMOW}$, the $\delta^{18}O$ composition of the vein cement corresponds to fluid temperatures of up to 95°C. These temperatures are two high considering that the section is still in the stability field of opal-CT, thereby limiting temperatures to <80°C (Keller and Isaacs, 1985). The temporary injection of hot fluid from deeper structural levels is unlikely because these veins lack any connection to continuous fluid conduits. Provided the low $\delta^{18}O$ composition of vein-filling quartz is not caused by sample impurities, the $\delta^{18}O_{SMOW}$ composition of the solution must have been heavier than -0.7‰. The ingression of meteoric water into the formation is unlikely considering that present-day formation water has positive $\delta^{18}O_{SMOW}$ values consistent with diagenetically altered basinal fluid. Quartz veins do not contain fluid inclusions suitable for microthermometry that would allow resolution of this ambiguity. It is noteworthy that Behl and Smith (1992) observed a similar depletion in ^{18}O in chalcedonic quartz, with a difference of 8 to 9‰ between pairs of opal-CT and chalcedonic quartz.

Baroque dolomite veins (F3)

The stable isotopic composition of F3 baroque dolomite veins at Arroyo Burro Beach is distinctly different from F1 dolomicrite, with $\delta^{18}O_{PDB}$ -6 to -7.5‰ and with $\delta^{13}C$ +4 to +9‰ (Figure 10). Winter and Knauth (1992) analyzed dolomite veins from Carpinteria, also shown in Figure 10, with an intermediate stable isotopic composition between F1 and F3 veins, which suggests continuous dolomite vein cementation.

The overall trend in carbon and oxygen isotopic composition toward isotopically lighter values from F1 to F3 veins is likely to reflect thermocatalytic organic-matter diagenesis during burial (Figure 10). The $\delta^{13}C$ composition of carbonate precipitated in organic-rich sediments typically follows a trend leading initially toward heavy carbon, characteristic of microbial methanogenesis, and back to lighter carbon derived from organic matter during thermal decarboxylation (Claypool and Kaplan, 1974; Winter and Knauth, 1992). At the same time, $\delta^{18}O$ values decrease continuously due to the increase in temperature.

The oxygen isotopic trend within the data set of F3 baroque dolomite veins at Arroyo Burro Beach deviates from the typical burial trend, however. The $\delta^{18}O$ composition shifts toward heavier values with continued dolomite precipitation, while still becoming more depleted in ^{13}C. Stripping the fluid of CO_{2gas} would deplete the fluid in ^{16}O but because of mass balance reasons even more so in ^{12}C, which is not seen in the record. More plausible is an enrichment in ^{18}O of the fluid due to dissolution–precipitation of low temperature phases at higher temperature. An enrichment in ^{18}O is consistent with the measured $\delta^{18}O$ composition of present-day formation water.

Two mineral systems, dolomite and silica phases, underwent dissolution and reprecipitation. Dissolution–

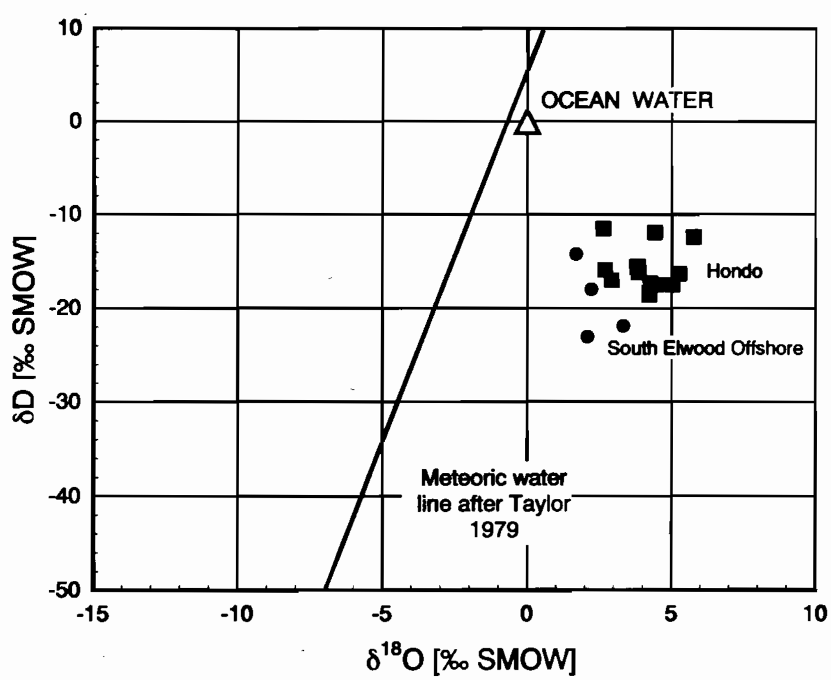

Figure 11: Oxygen versus hydrogen isotopic composition of Monterey formation water from the Hondo and South Elwood oil fields. Data are listed in Table 5.

Oil field/Platform/Well	$\delta^{18}O_{SMOW}$	δD_{SMOW}
South Elwood/Holly 3120-9	1.70	-14.2
South Elwood/Holly 3242-12	2.23	-18.0
South Elwood/Holly 3242-17	2.09	-23.1
South Elwood/Holly 3242-18	3.34	-21.9
Hondo/Hondo H-18	5.26	-16.3
Hondo/Hondo H-31	3.86	-16.2
Hondo/Hondo H-33	4.42	-11.9
Hondo/Hondo H-35	5.76	-12.4
Hondo/Hondo H-37	4.26	-17.3
Hondo/Hondo H-23	5.02	-17.5
Hondo/Harmony HA-3	4.46	-17.5
Hondo/Harmony HA-5	4.23	-18.6
Hondo/Harmony HA-6	3.83	-15.5
Hondo/Harmony HA-8	3.81	-15.6
Hondo/Harmony HA-12	2.70	-15.9
Hondo/Harmony HA-13	2.93	-17.0
Hondo/Harmony HA-16	2.64	-12.0

Table 5: Stable isotopic composition of Monterey Formation water from Hondo and South Elwood Offshore oil fields.

precipitation of dolomite under closed system conditions would enrich the fluid in ^{18}O but also in ^{13}C, i.e. increase the $\delta^{13}C$ composition of the fluid. Enrichment in ^{18}O without affecting the $\delta^{13}C$ trend toward lighter values due to thermal decarboxylation could be due to dissolution–recrystallization of opal-A to opal-CT and of opal-CT to quartz. The large component of silica phases in the Monterey Formation suggests that silica dissolution–reprecipitation is the main contributing factor to positive $\delta^{18}O$ values as analyzed in present-day formation water.

Calcite veins (F4)

A shift in the fluid oxygen isotopic composition toward heavier values is also suggested by the $\delta^{18}O_{PDB}$ composition of F4 calcite veins that ranges between -5 and -6.5‰. Assuming an intermediate $\delta^{18}O_{SMOW}$ value of present-day formation water of +3‰ gives a calcite precipitation temperature of about 65°C. This is the maximum temperature still compatible with single-phase fluid inclusions in this vein cement. Higher $\delta^{18}O_{SMOW}$ values of present-day formation water of up to +6‰ may be explained by the fact that formation water is partly sampled from sections that are in the quartz diagenetic stage. These fluids have therefore experienced more water-rock interaction than can be expected for the Arroyo Burro Beach section that has not exceeded opal-CT stability conditions.

The $\delta^{13}C_{PDB}$ composition of F4 calcite veins at Arroyo Burro Beach is around +1‰, distinctly lighter than any dolomite cement. Possible carbon sources are calcite shell tests, dolomite, CO_2 from thermocatalytic degradation of organic matter, and organic acids. Carbon derived predominantly from dolomite is too heavy, and from thermogenic CO_2, typically between -10 and -25‰$_{PDB}$ (Longstaffe, 1989), too light. The carbon isotopic composition of organic acids is highly variable (Franks and others, 1997). Shell tests of foraminifera are abundant in porcelanite and show evidence for partial or complete dissolution. Isaacs (1984) analyzed calcite from porcelanite containing foraminifera tests, obtaining $\delta^{13}C_{PDB}$ values of -2 to -3‰ and $\delta^{18}O_{PDB}$ values of 0 to -6‰. Furthermore, shell tests are also a likely source of Ca^{2+}, rather than dolomite which would release excess Mg^{2+} into solution. Calcite tests are thus a likely source for carbon in F4 calcite veins. The somewhat more positive $\delta^{13}C_{PDB}$ composition of F4 calcite veins of +1‰ may be explained with a component of heavy carbon from dolomite.

From Isaacs' (1984) data it is apparent that calcite shell tests in siliceous mudstone bypassed the zone of bacterial methanogenesis during recrystallization, undergoing a diagenetic evolution separate from dolomite.

DISCUSSION

Vein cementation in relation to host rock and organic matter diagenesis

Veins at Arroyo Burro Beach have the following characteristics:

1. Multiple vein systems formed by repeated fracture opening and complete cementation.
2. Initial fracture opening and brecciation that allowed rotation and translation of host rock fragments. Fracture opening continued after initial cementation by crack-seal.
3. Clustering of veins ultimately led to rock fragmentation.
4. Vein cementation correlates with host rock pore cementation and alteration: F1 dolomicrite veins formed synchronously with or immediately after authigenic dolostone formation; F2 quartz and F3 baroque dolomite vein cementation can be correlated with quartz and dolomite pore cementation in the host rock; F4 calcite vein cementation appears to have accompanied dissolution of calcite tests and organic matter catagenesis in the surrounding country rock. These correlations between vein cementation and country rock alteration suggest a genetic link between both processes.
5. Host rock alteration is typically enhanced in rock fragments contained in veins.

The similarity between the cement sequences in the host rock and in fractures may imply one of the following cause-effect relations: 1.) Host rock diagenetically altered due to fluid entering the host rock from fractures. 2.) Fluids migrate through porous host rock and fractures alike, precipitating the same phases in both places. 3.) Cementation of fractures follows or accompanies burial diagenetic replacement in the host rock, with local mass transfer from the host rock into fractures by diffusive processes or by slow seepage of pore fluid. Diagenetic alteration in case 2. and 3. are regional processes whereas in case 1., diagenesis is localized next to fractures. In case 2., the wall rock is relatively open to fluid flow unlike case 3. where the wall rock is relatively closed. Case 3. may still allow mass transfer out of the host rock into the fractures, either by diffusive mass transfer or by migration of fluid.

Because no gradient in host rock alteration is observed beyond a few microns away from fracture surfaces, case 1. is rejected. The alteration sequence observed in the host rock is rather a process of regional extent. Case 2. is rejected as well because the transformation of opal-CT to quartz in porcelanite and dolomitic porcelanite appears to occur in a relatively closed system as inferred by Behl and Garrison (1994) and Behl (1998) based on mass-balance arguments. An exception are opal-CT and quartz cherts with clear evidence for silica advection (Behl and Garrison, 1994; Behl, 1998). We may therefore envision case 3., with host rock alteration as a regional process of burial diagenesis, controlling fracture cementation through local mass transfer out of the host rock.

Local mass transport from the country rock into the fracture system is consistent with the observation that fracture generations of distinct composition are restricted to specific types of host rock. Fluid flow within fractures may redistribute solutes over larger distances. Evidence for fluid flow has been observed through laminated dolomicrite (Plate 2h). Upward fluid flow may also explain apparent addition of silica in F2 veins and removal of silica in F3 veins. Silica dissolved during F3 dolomite recrystallization may be transported upward and precipitated farther upsection in fractures that are at the stage of F2 quartz vein cementation and replacement. Silica is thus transported from sites that are more advanced in burial diagenesis, i.e. lower in the section, to sites higher up in the section.

Repeated fracturing, fracture clustering, the correlation between fracturing and host rock alteration, and the enhanced alteration in fragments could be explained if host rock diagenesis favored, enhanced, or induced fracturing and if fractures provided a positive feedback to host rock alteration.

Possible diagenetic processes which may accompany fracture cementation and which may become enhanced through fracturing are difficult to identify because the Monterey Formation underwent a complex diagenetic evolution during burial. This complex evolution is due to a 'reactive' initial sediment composition: 1.) a large component of organic matter; 2.) metastable phases such as biogenic silica; 3.) hydrous phases such as opal-A and clay which release fluid during diagenesis, thus favoring dissolution–precipitation reactions; and 4.) a fine grain size providing a large surface to volume ratio for surface reactions. Complexity is also added by precipitation of metastable phases such as opal-CT and non-stoichiometric dolomite during early diagenesis.

Diagenesis of the Monterey Formation, however, may be retarded by the low matrix permeability, typically <0.1md (Crain and others, 1985; Roehl and Weinbrandt, 1985; Isaacs and Petersen, 1987; MacKinnon, 1989), restricting advective mass transfer. In this case, fracturing may be expected to act as a catalyst for any non-conservative diagenetic reaction that requires addition or removal of dissolved species. An example would be the illitization of smectite, requiring addition of K^+ and removal of Na^+, Ca^{2+}, Mg^{2+}, Fe^{3+}, and H_20, assuming Al^{3+} is conserved (Boles and Franks, 1979). Although this reaction involves dehydration of the solid phase, removal of released water would not be expected to enhance the reaction under constant pressure conditions because the system can be assumed to be water saturated.

Release of fluid may increase the pore fluid pressure, however. In a closed system undergoing burial with a geobaric gradient dP/dT_{burial}, a dehydration reaction $A \rightarrow B+H_2O$ with $\Delta V_{reaction}$ positive may locally increase the pore fluid pressure gradient. If $dP/dT_{reaction}$ of the phase boundary is higher than the geobaric gradient before onset of the dehydration reaction, then the reaction would not go to completion. Instead, the rate of dehydration with increasing burial would adjust so that dP/dT_{burial} follows $dP/dT_{reaction}$ until the reactant is depleted. Creation of a fracture such as by hydraulic fracturing, however, could open the system, thus leading to a drop in fluid pressure. The dehydration reaction may then spontaneously go to completion.

In addition to releasing structural water during diagenesis, collapse of framework minerals by dissolution and concomitant compaction may also increase the pore fluid pressure, thus affecting diagenetic reactions, provided fluid drainage is inhibited. Because the solubility of silica slightly increases with increasing pressure (Walther and Helgeson, 1977), dissolution would be favored during dissolution of framework-supporting silica phases. Fracturing and resulting fluid drainage, on the other hand, would rather impede dissolution of the framework and may lead to silica precipitation in the fracture during upward flow.

The response of dissolved carbonate to a pressure increase by framework collapse under constant P_{CO2} would be opposite to that of quartz (Bruton and Helgeson, 1983). Any enhancement of carbonate dissolution due to a decrease in pore pressure adjacent to a fracture would likely be overwhelmed by the drop in P_{CO2} favoring carbonate precipitation. For most geobaric gradients, the drop in P_{CO2} during upward fluid flow in fractures outweighs the increase in carbonate solubility with decreasing temperature thus favoring carbonate precipitation (Lundegard and Land, 1986; Eichhubl, 1997). Pressure effects on mineral stability and diagenesis associated with fracture formation would thus be small, with exception of changes in fluid pressure controlling P_{CO2}.

A pronounced effect of fracturing on host rock diagenesis may be expected during late diagenesis and catagenesis of organic matter. The thermal breakdown of organic matter during late diagenesis produces water, CO_2, CH_4, H_2S, organic acids, bitumen, and, with beginning catagenesis, a liquid oil phase while CO_2 generation starts to decrease (Hunt, 1996, p. 187; Lewan and Fisher, 1994). The volume of organic matter and compounds derived from kerogen expands during catagenesis by up to 15% (Ungerer and others, 1983). Drainage of the fluid phases and the associated drop in fluid pressure are expected to enhance catagenesis of organic matter. Advection of heat with expulsion of fluid out of the source rock causing a drop in temperature may cancel this effect in part. Host rock carbonate dissolution may be enhanced, however, next to fractures through organic acid generation in the matrix, reaction of organic acid with host rock carbonate, and advective transport of complexed cations out of the host rock.

Organic acid such as acetic acid reacts with carbonate minerals through the reaction

$$CH_3COOH + MeCO_3 \rightarrow MeCH_3COO^+ + HCO_3^-$$

where Me stands for any divalent metal. Carbonate precipitation in the fracture is controlled by the organic acid concentration in the aqueous fluid and CO_2 partial pressure. Carbon dioxide is produced directly from kerogen during catagenesis and through degradation of organic acids

(Lundegard and Land, 1986; Lundegard and Kharaka, 1994). At high organic acid concentrations, i.e. >0.14 m acetic acid at 60°C (Lundegard and Land, 1989), organic acid acts as a buffer to added CO_2 resulting in carbonate precipitation (Surdam and Crossey, 1985). At lower organic acid concentrations, carbonate would be precipitated with decreasing P_{CO2} as expected during upward flow of the aqueous solution.

Fluid pressure and fluid flow in the fracture system could cause subtle changes in carbonate dissolution–precipitation conditions by controlling the influx of organic acid, affecting the residence time of organic acid and thus its degradation in the fracture system, and through changes in P_{CO2}. Focusing of fluid toward fractures would enhance carbonate dissolution in the surrounding host rock and cementation in the fractures.

Organic acid concentrations in present-day formation water of the Monterey Formation are exceptionally high, with average acetate concentrations of about 2,500 mg/L and maximum concentrations of 5,800 mg/L (S. G. Franks, Arco, written communication, 1996). Lewan and Fisher (1994) explained the high organic acid concentration by the early onset of catagenesis of Monterey kerogen reducing early loss in organic acid during diagenesis as compared to other source rocks which undergo catagenesis at higher temperatures and deeper burial. The concentration of organic acids in formation water of the San Joaquin basin reaches a maximum between 80 and 100°C (Fisher and Boles, 1990; Lundegard and Kharaka, 1994) although acetate concentrations may exceed 1,000 mg/L at formation temperatures as low as 30°C (S. G. Franks, oral communication, 1996). Thermal decarboxylation decreases organic acid concentration at temperatures generally above 140°C, while microbial metabolism decreases organic acid generation by decomposition into CO_2 and CH_4 at temperatures below 80°C (Lundegard and Kharaka, 1994).

The high organic acid concentration measured in Monterey formation water makes it likely that organic acids mediated dissolution and precipitation of dolomite and calcite in F3 and F4 veins. Alternation of dissolution and precipitation in these veins would be difficult to explain by temperature or by pressure variations and corresponding P_{CO2} variations alone. F3 veins and part of F4 veins are not connected to large faults where seismic fault slip would allow significant and rapid changes in fluid temperature and pressure.

In particular, the generation of organic acid *in situ* from organic matter and/or hydrocarbons contained in the host rock can explain pervasive dolomite and calcite dissolution in the host rock on a regional scale as opposed to localized dissolution adjacent to fractures by exotic fluids. Flow of pore fluid may transport Ca^{2+} and Mg^{2+} as organic complexes into fractures where changes in organic acid and CO_2 concentrations would control carbonate precipitation in the way outlined above.

The inferred temperature of F3 baroque dolomite and in particular of F4 calcite vein cementation of about 60°C also appears to coincide with the expected increase in organic acid generation. In this temperature range, it is also feasible that cementation is favored by microbial decomposition of organic acid generating CO_2 which, due to the organic acid buffer, precipitates carbonate.

The temporal link between F3 and F4 vein cementation and organic matter is also apparent from the carbon isotopic shift toward lighter values, as discussed in the previous section. The involvement of organic acids in carbonate cementation, however, is difficult to ascertain using carbon isotopes because of the variable carbon isotopic composition of organic acids (Franks and others, 1997).

A possible effect of organic acids on silica dissolution and precipitation in F2 quartz veins is less obvious: The increase in silica solubility due to complexation with organic ligands is negligible under high silica concentrations, i.e. when saturated with respect to opaline silica, and small under concentrations in equilibrium with quartz (Fein and Hestrin, 1994). Silica diagenesis in siliceous dolostone could be enhanced by dissolution of framework dolomite, however, thus opening the system to fluid flow that may favor dissolution of metastable opal-CT. Dolomite dissolution could be caused by organic acid generation. Dolomite dissolution is, in fact, observed in F2 breccias (Plate 1f).

Alternatively, or in addition to effects of organic acid production, F2 vein cementation may be controlled by factors controlling the kinetics of opal-CT dissolution and quartz precipitation. The opal-CT to quartz transformation in dolostone apparently occurs at lower temperatures than in clay-bearing porcelanite which is still in the opal-CT stage at Arroyo Burro Beach. Clays retard the transformation of opal-A to opal-CT but have the opposite effect on the transformation of opal-CT to quartz (Isaacs, 1982; Williams and others, 1985). The lower clay content in dolostone is therefore not expected to further precipitation of quartz in F2 veins.

Kastner and others (1977) and Kastner and Gieskes (1983) reported that nuclei of magnesium hydroxide facilitate opal-CT precipitation. Opal-CT experimentally grown with addition of $Mg(OH)_2$ has a higher degree of ordering as compared to opal-CT grown without this addition. The better ordered opal-CT may convert to quartz at lower temperatures because fewer recrystallization steps are required to attain higher ordering before conversion to quartz (Kastner and Gieskes, 1983). The early opal-CT to quartz transformation seen in siliceous dolostone may therefore be the result of a more conducive environment for opal-CT precipitation earlier in the diagenetic history, but otherwise not different from the opal-CT to quartz transformation in porcelanite. Higher initial ordering of opal-CT may also explain the early-CT to quartz transformation in opal-CT chert spheroids (R. J. Behl, California State Univ. Long Beach, oral communication, 1996). Opal-CT chert spheroids form in clay-poor layers by local addition of silica (Behl, 1992), which may lead to higher initial ordering as compared to the closed-system formation of opal-CT in porcelanite.

F2 and F3/F4 veins have in common that the diagenetic alteration of the host rock and that of breccia fragments are similar although strongly enhanced in breccia fragments, and that reaction halos around fractures are typically absent. The similarity appears surprising if the diagenetic processes accompanying F2 and F3/F4 cementation are different, i. e. opal-CT dissolution during F2 quartz vein cementation, and carbonate dissolution, mediated by organic acid generation, during F3/F4 dolomite and calcite vein cementation. Both processes have in common, however, that they are triggered by the instability of metastable phases which are main constituents of the host rock—opal-CT and organic matter.

Also, both processes release fluid with the tendency to flow out of the host rock into fractures.

Focusing of fluid along fractures would favor opal-CT dissolution in host rock fragments because large fluid volumes are available for dissolution–precipitation reactions. Opal-CT dissolution would proceed even during upsection flow and concomitant cooling of fluid as long as quartz precipitation in other parts of the vein system kept the solution undersaturated with respect to opal-CT. Dissolution of the wallrock, on the other hand, would not be enhanced because the higher pressure in the wallrock prevents fluid flow back into the host rock. Instead, opal-CT dissolution and quartz precipitation in the wallrock would proceed at a much slower rate, presumably largely by diffusive mass transfer and slow fluid flow through the matrix of the low-permeability host rock. Enhanced alteration of host rock fragments would be expected to occur as soon as host rock fragments are sufficiently separated from the wallrock to shut off fluid seepage from the wallrock into the fracture, allowing fluid to enter the host rock fragment.

The same principles may apply to alteration of fragments in F3 and F4 veins. Organic matter is the unstable host rock component in this case, with organic acid generation possibly controlling carbonate dissolution. Fluid seepage out of the country rock and focusing of fluid flow in fractures may explain enhanced alteration of breccia fragments. Carbonate dissolution and precipitation are controlled by CO_2 generation from kerogen and organic acid breakdown and changes in P_{CO2} due to fluid pressure variations. The lack of alteration halos is again explained by a higher fluid pressure in the wallrock as compared to open fractures, thus inhibiting influx of fluid into the wallrock.

Implications of vein formation on fractured reservoir properties of the Monterey Formation

Predicting reservoir properties in the Monterey Formation requires prediction of the occurrence of open fractures. The density of fractures in the Monterey Formation correlates only weakly with folding but strongly with host rock composition and diagenetic grade (Redwine, 1981; Grivetti, 1982; Belfield, 1983; Narr, 1991; Gross, 1995). Similarly, no correlation is noticed between vein occurrence of F4 vein sets and location of fold hinges at Arroyo Burro Beach: F4 veins are observed within the limbs of mesoscale folds rather than in fold hinges where bending may be expected to contribute to fracture formation (Murray, 1968; Stearns and Friedman, 1972; Narr, 1991). No correlation with folds is observed and expected for F1 to F3 veins which predate folding.

Characteristic of Monterey veins, in particular of calcite veins, is their clustering (Figures 4 to 9). As demonstrated by Fischer at al. (1995), fracture formation by changes in pore pressure or confining stress leads to equal fracture spacing in layered media. Shielding through stress changes adjacent to fracture walls, accomplished by pore fluid drainage out of the wall rock and by stress relaxation, inhibits formation of closely spaced parallel fractures. Fracture formation by changes in pore pressure or confining stress thus leads to equally spaced fracture sets of some characteristic spacing distance. The cut-off at 5 cm for dolostone and 2 cm for porcelanite maybe explained by this shielding effect, preventing formation of fractures closer than this minimum spacing.

The clustering at fracture spacings above 5 and 2 cm, respectively, indicates that local factors affect fracture spacing rather than uniform far field extension. We speculate that local mass transfer adjacent to fractures, evoked in the previous section to explain vein cementation, may change either the mechanical properties of the host rock or the local stress state facilitating formation of closely-spaced subparallel veins or both. In both these cases, the distribution of veins would follow a diffusion profile adjacent to pre-existing fractures.

If local mass transport contributes to the formation of vein clusters, then fluid flow in fractures would be self-enhancing, creating more fracture space adjacent to existing fluid conduits with increasing fluid flow and increasing size of the fracture network. This self-enhancement will be counteracted by cementation. The interplay between fracture formation and cementation, both controlled by fluid flow, may lead to cyclic formation and cementation of fracture systems similar to those observed in the Monterey Formation.

The observed clustering of veins suggests that the highest density of fractures is expected adjacent to faults, a finding consistent with measurements of joint spacing in the Monterey Formation (D. L. Lockman, Exxon, Thousand Oaks, oral communication, 1996). Fracture permeability is controlled by the degree of cementation. The observed correlation of vein cements with the diagenetic evolution of the host rock suggests that fracture cementation depends in part on the stability or reactivity of the host rock for diagenesis for given temperature, pressure, and fluid composition conditions. The more stable the host rock, the more likely the fractures remain uncemented and available for fluid flow. The diagenetically most stable host rock composition in the Monterey Formation is quartz chert which is consistent with the superior reservoir properties of this rock type.

CONCLUSIONS

Repeated fracturing and cementation lead to a distinct sequence of quartz and carbonate veins in the Monterey Formation along the Santa Barbara coast:

Dolomicrite veins form during early diagenesis in the zone of microbial methanogenesis, postdating formation of the hosting authigenic dolostone. Quartz cementation of the next fracture generation, developed in siliceous dolostone, appears to be synchronous with opal-CT dissolution and quartz precipitation in the host rock. Quartz vein formation is followed by two carbonate vein generations, an earlier cemented by baroque dolomite and a later one by calcite. Opening and cementation of these veins is interpreted to follow dissolution of host rock carbonate, presumably in response to organic acid generation during organic matter diagenesis and beginning catagenesis. Precipitation of carbonate vein cement and localized dissolution and corrosion of breccia fragments in these veins may be explained by changes in organic acid concentration and in CO_2 partial pressure.

Both opal-CT dissolution during quartz vein cementation and organic matter diagenesis during carbonate vein cementation are considered part of the burial diagenesis of the sequence and not a localized phenomenon around fractures. In both cases, it appears that fluid flow out of the wallrock inhibits extensive wallrock alteration around fractures, whereas isolated host rock fragments contained in these fractures show enhanced corrosion, dissolution, and replacement. Fluid flow during quartz vein cementation may be caused by the collapse of framework opal-CT and resulting compaction, augmented by release of structural water. Fluid flow during dolomite and calcite vein cementation is explained by the generation of fluid during organic matter diagenesis and beginning catagenesis.

Characteristic of calcite veins is their clustering rather than equal spacing, that is typically observed for systematic joint sets. Clustering of fractures ultimately leads to brecciation of the wall rock. Clustering indicates some self-amplification process, i.e. fractures favoring formation of other, closely spaced sub-parallel fractures. Because mechanical joint interaction tends to oppose growth of sub-parallel fractures, local mass transfer out of the host rock into fractures may be responsible for changes in rock mechanical properties or in stress state favoring formation of vein clusters.

ACKNOWLEDGMENTS

This work benefited from discussions with Michael Gross, Wendy Bartlett, Rick Behl, Rick Sibson, and Steve Franks. James Elliot introduced P.E. to vein formation and brecciation in the Monterey Formation. Mobil and Exxon provided formation water samples for isotopic analyses for which Arco provided logistical and financial support. Art Sylvester reviewed an early version of this manuscript. This research was funded in part by NSF grant EAR-93-04581 and a grant from the Geological Society of America.

REFERENCES

Arends, R. G., and Blake, G. H., 1986, Biostratigraphy and paleoecology of the Naples Bluff coastal section based on diatoms and benthic foraminifera, in, Casey, R. E., and Barron, J. A. (eds.), Siliceous microfossil and microplancton of the Monterey Formation and modern analogs: SEPM Pacific Section Special Publication, vol. 45, p. 121-135.

Barron, J. A., 1986, Updated diatom stratigraphy for the Monterey Formation of California, in: Casey, R. E., and Barron, J. A., eds., Siliceous microfossil and microplancton of the Monterey Formation and modern analogs: SEPM Pacific Section Special Publication, vol. 45, p. 105-119.

Behl, R. J., 1992, Chertification in the Monterey Formation of California and Deep-Sea Sediments of the West Pacific [Ph.D. Thesis]: University of California, Santa Cruz, 287 p.

Behl, R. J., and Garrison, R. E., 1994, The Origin of Chert in the Monterey Formation of California (USA), in: Iijima, A., ed., Proceedings of the 29th International Geological Congress, Part C, p. 101-132

Behl, R. J., and Smith, B. M., 1992, Silicification of Deep-Sea Sediments and the Oxygen Isotopic Composition of Diagenetic Siliceous Rocks from the Western Pacific, Pigafetta and East Mariana Basins, Leg 129: Proceedings of the Ocean Drilling Program, Scientific Results, vol. 129, p. 81-117.

Behl, R. J., 1998, Relationships Between Silica Diagenesis, Deformation, and Fluid Flow in Monterey Formation Cherts: this volume.

Belfield, W. C., Helwig, J., La Pointe, P., and Dahleen, W. K., 1983, South Ellwood Oil Field, Santa Barbara Channel, California, a Monterey Formation Fractured Reservoir, in: Isaacs, C. M., and Garrison, R. E., eds., Petroleum Generation and Occurrence in the Miocene Monterey Formation, California: Los Angeles, Pacific Section Society of Economic Paleontologists and Mineralogists, p. 213-221.

Boles, J. R., and Franks, S. G., 1979, Clay diagenesis in Wilcox sandstone of southwest Texas: implications of smectite diagenesis on sandstone cementation: Journal of Sedimentary Petrology, vol. 49, p. 55-70.

Boles, J. R., and Franks, S. G., 1979, Clay diagenesis in Wilcox sandstone of southwest Texas: implications of smectite diagenesis on sandstone cementation: Journal of Sedimentary Petrology, vol. 49, p. 55-70.

Bruton, C. J., and Helgeson, H. C., 1983, Calculation of the Chemical and Thermodynamic Consequences of Differences Between Fluid and Geostatic Pressure in Hydrothermal Systems: American Journal of Science, vol. 283-A, p. 540-588.

Claypool, G. E., and Kaplan, I. R., 1974, The Origin and Distribution of Methane in Marine Sediments, in: Kaplan, I. R., ed., Natural Gases in Marine Sediments: New York, Plenum Press, p. 99-139.

Compton, J. S., 1988, Sediment Composition and Precipitation of Dolomite and Pyrite in the Neogene Monterey and Sisquoc Formations, Santa Maria Basin Area, California, in:, V., and Baker, P. A., eds., Sedimentology and Geochemistry of Dolostones: Tulsa, Society of Economic Paleontologists and Mineralogists Special Publication, vol. 43, p. 53-64.

Compton, J. S., 1991a, Porosity reduction and burial history of siliceous rocks from the Monterey and Sisquoc Formation, Point Pedernales area, California: Geological Society of America Bulletin, vol. 103, p. 625-636.

Compton, J. S., 1991b, Origin and Diagenesis of Clay Minerals in the Monterey Formation, Santa Maria Basin Area, California: Clay and Clay Minerals, vol. 39, p. 449-466.

Crain, W. E., Mero, W. E., and Patterson, D., 1985, Geology of the Point Arguello Discovery: AAPG Bulletin, vol. 69, p. 537-545.

DePaolo, D. J., and Finger, K. L., 1991, High-resolution strontium-isotope stratigraphy and biostratigraphy of the Miocene Monterey Formation, central California: Geological Society of America Bulletin, vol. 103, p. 112-124.

Dibblee, T. W., 1966, Geology of the Central Santa Ynez Mountains, Santa Barbara County, California: California Division of Mines and Geology Bulletin, vol. 186, 99 p.

Dibblee, T. W. Jr., 1986a, Geologic Map of the Santa Barbara Quadrangle, Santa Barbara County, California, 1:24.000: Santa Barbara, Dibblee Foundation.

Dibblee, T. W. Jr., 1986b, Geologic Map of the Goleta Quadrangle, Santa Barbara County, California,

1:24.000: Santa Barbara, Dibblee Foundation.
Dibblee, T. W. Jr., 1987, Geologic Map of the Dos Pueblos Quadrangle, Santa Barbara County, California, 1:24.000: Santa Barbara, Dibblee Foundation.
Donnellan, A., Hager, B. H., King, R. W., and Herring, T. A., 1993, Geodetic Measurement of Deformation in the Ventura Region, Southern California: Journal of Geophysical Research, vol. 98, p. 21727-21739.
Dumont, M.P., 1989, The Monterey Formation and biostratigraphy: An overview, in: MacKinnon, T., and Randall, J.W., eds., Oil in the California Monterey Formation: Field trip guidebook T311 1GC 1989, American Geophysical Union, p. 28-32.
Echols, R. J., 1994, Biostratigraphy of the Luisian and Mohnian Stages Between Santa Barbara and Gaviota, California, in: Hornafius, S. J., ed., Field Guide to the Monterey Formation Between Santa Barbara and Gaviota, California: Bakersfield, AAPG Pacific Section, p. 29-44.
Eichhubl, P., 1997, Scale, Rates, and Timing of Fracture-Related Fluid Flow in the Miocene Monterey Formation, Coastal California [Ph. D. dissertation]: University of California, Santa Barbara, 298 p.
Feary, D. A., Davies, P. J., Pigram, C. J., and Symonds, P. A., 1991, Climatic evolution and control on carbonate deposition in northeast Australia: Palaeogeography, Palaeoclimatology, Palaeoecology, vol. 89, p. 341-361.
Feigl, K. L., Agnew, D. C., Bock, Y., Dong, D., Donnellan, A., Hager, B. H., Herring, T. A., Jackson, D. D., Jordan, T. H., King, R. W., Larsen, S., Larson, K. M., Murrey, M. H., Shen, Z., and Webb, F. H., 1993, Space Geodetic Measurement of Crustal Deformation in Central and Southern California, 1984-1992: Journal of Geophysical Research, vol. 98, p. 21677-21712.
Fein, J. B., and Hestrin, J. E., 1994, Experimental studies of oxalate complexation at 80°C: Gibbsite, amorphous silica, and quartz solubilities in oxalate-bearing fluids: Geochimica et Cosmochimica Acta, vol. 58, p. 4817-4829.
Fischer, M. P., Gross, M. R., Engelder, T., and Greenfield, R. J., 1995, Finite-element analysis of the stress distribution around a pressurized crack in a layered elastic medium: implications for the spacing of fluid-driven joints in bedded sedimentary rock: Tectonophysics, vol. 247, p. 49-64.
Fisher, J. B., and Boles, J. R., 1990, Water-rock interaction in Tertiary sandstones, San Joaquin Basin, California, U.S.A.; diagenetic controls on water composition: Chemical Geology, vol. 82, p. 83-101.
Föllmi, K. B., and Garrison, R. E., 1991, Phosphatic Sediments, Ordinary or Extraordinary Deposits? The Example of the Miocene Monterey Formation (California), in: Müller, D. W., McKenzie, J. A., and Weissert, H., eds., Controversies in Modern Geology: London, Academic Press, p. 55-84.
Franks, S. G., Boles, J. R., Fincannon, A. L., Freeman, K. H., Holba, A. G., and Jordan, E. D., 1997, Carbon Isotopic Composition of Organic Acids in Oilfield Waters, San Joaquin Basin, California: AAPG Annual Convention Official Program, vol. 6, p. A37.
Grimm, K. A., and Orange, D. L., 1997, Synsedimentary fracturing, fluid migration, and subaqueous mass wasting: intrastratal microfractured zones in laminated diatomaceous sediments, Miocene Monterey Formation, California, U.S.A.: Journal of Sedimentary Research, vol. 67, p. 601-613.
Grivetti, M. C., 1982, Aspects of Stratigraphy, Diagenesis, and Deformation in the Monterey Formation Near Santa Maria-Lompoc, California [Master's Thesis]: University California, Santa Barbara, 155 p.
Gross, M. R., 1993, The origin and spacing of cross joints: examples from the Monterey Formation, Santa Barbara Coastline, California: Journal of Structural Geology, vol. 15, p. 737-751
Gross, M. R., 1995, Fracture partitioning: Failure mode as a function of lithology in the Monterey Formation of coastal California: Geological Society of America Bulletin, vol. 107, p. 779-792.
Gross, M. R., and Engelder, T., 1995, Strain accommodated by brittle failure in adjacent units of the Monterey Formation, U.S.A.: scale effects and evidence for uniform displacement boundary conditions: Journal of Structural Geology, vol. 17, p. 1303-1318.
Hornafius, J.S., 1985, Neogene Tectonic Rotation of the Santa Ynez Range, Western Transverse Ranges, California, Suggested by Paleomagnetic Investigation of the Monterey Formation: Journal of Geophysical research, vol. 90, p. 12503-12522.
Hornafius, J. S., Luyendyk, B. P., Terres, R. R., and Kamerling, M. J., 1986, Timing and extent of Neogene tectonic rotation in the western Transverse Ranges, California: Geological Society of America Bulletin, vol. 97, p. 1476-1487.
Hornafius, S. J., 1994a, Correlation of Volcanic Ashes in the Monterey Formation Between Naples Beach and Gaviota Beach, California, in: Hornafius, S. J., ed., Field Guide to the Monterey Formation Between Santa Barbara and Gaviota, California: Bakersfield, AAPG Pacific Section, p. 45-58.
Hornafius, S. J., 1994b, Field Trip Log to the Monterey Formation Between Santa Barbara and Gaviota, California, in: Hornafius, S. J., ed., Field Guide to the Monterey Formation Between Santa Barbara and Gaviota, California: Bakersfield, AAPG Pacific Section, p. 107-123.
Hornafius, S. J., 1994c, Overview of the Stratigraphy of the Monterey Formation Along the Coastline Between Santa Barbara and Gaviota, California, in: Hornafius, S. J., ed., Field Guide to the Monterey Formation Between Santa Barbara and Gaviota, California: Bakersfield, AAPG Pacific Section, p. 1-15.
Hsu, K. J., Kelts, K., and Valentine, J. W., 1980, Resedimented Facies in Ventura Basin, California, and Model of Longitudinal Transport of Turbidity Currents: AAPG Bulletin, vol. 64, p. 1034-1051.
Huftile, G. J., and Yeats, R. S., 1995, Convergence rates across a displacement transfer zone in the western Transverse Ranges, Ventura basin, California: Journal of Geophysical Research, vol. 100, p. 2043-2067.
Hunt, J. M., 1996, Petroleum Geochemistry and Geology:

New York, Freeman, 743 p.
Isaacs, C. M., 1980, Diagenesis in the Monterey Formation examined laterally along the coast near Santa Barbara, California [Ph.D. dissertation]: Stanford Univ., 329 p.
Isaacs, C. M., 1981a, Lithostratigraphy of the Monterey Formation, Goleta to Point Conception, Santa Barbara coast, California, in: Isaacs, C. M., ed., Guide to the Monterey Formation in the California coastal area, Ventura to San Luis Obispo, AAPG Pacific Section, vol. 52, p. 9-24.
Isaacs, C. M., 1981b, Outline of diagenesis in the Monterey Formation examined laterally along the Santa Barbara coast, California, in: Isaacs, C. M., ed., Guide to the Monterey Formation in the California coastal area, Ventura to San Luis Obispo, AAPG Pacific Section, vol. 52, p. 25-38.
Isaacs, C. M., 1981c, Field characterization of rocks in the Monterey Formation along the coast near Santa Barbara, California, in: Isaacs, C. M., ed., Guide to the Monterey Formation in the California coastal area, Ventura to San Luis Obispo, AAPG Pacific Section, vol. 52, p. 39-53.
Isaacs, C. M., 1981d, Porosity reduction during diagenesis of the Monterey Formation, Santa Barbara coastal area, California, in: Garrison, R. E., and Douglas, R. G., eds., The Monterey Formation and related siliceous rocks of California: Los Angeles, SEPM Pacific Section, p. 257-271.
Isaacs, C. M., 1982, Influence of rock composition on the kinetics of silica phase changes in the Monterey Formation, Santa Barbara area, California: Geology, vol. 10, p. 304-308.
Isaacs, C. M., 1983, Compositional variation and sequence in the Miocene Monterey Formation, Santa Barbara coastal area, California, in: Larue, D. K., and Steel, R. J., eds., Cenozoic marine sedimentation, Pacific margin, U.S.A.: Los Angeles, SEPM Pacific Section, p. 117-132.
Isaacs, C. M., 1984, Disseminated Dolomite in the Monterey Formation, Santa Maria and Santa Barbara Areas, California, in: Garrison, R. E., Kastner, M., and Zenger, D. H., eds., Dolomites of the Monterey Formation and Other Organic-Rich Units: Los Angeles, SEPM Pacific Section, p. 155-169.
Isaacs, C. M., and Petersen, N. F. 1987, Petroleum in the Miocene Monterey Formation, California, in: Hein, J. R., ed., Siliceous Sedimentary Rock-Hosted Ores and Petroleum, Van Nostrand Reinhold, New York, p. 83-116.
Jackson, P. A., and Yeats, R. S., 1982, Structural Evolution of Carpinteria Basin, Western Transverse Ranges, California: AAPG Bulletin, vol. 66, p. 805-829.
Kastner, M., and Gieskes, J. M., 1983, Opal-A to Opal-CT Transformation: A Kinetic Study, in: Ijima, A., Hein, J. R., and Siever, R., eds., Siliceous Deposits in the Pacific Region: Amsterdam, Elsevier, p. 211-227.
Kastner, M., Keene, J. B., and Gieskes, J. M., 1977, Diagenesis of siliceous oozes–I. Chemical controls on the rate of opal-A to opal-CT transformation–an experimental study: Geochimica et Cosmochimica Acta, vol. 41, p. 1041-1059.
Keller, M. A., and Isaacs, C. M., 1985, An Evaluation of Temperature Scales for Silica Diagenesis in Diatomaceous Sequences Including a New Approach Based on the Miocene Monterey Formation, California: Geo-Marine Letters, vol. 5, p. 31-35.
Levi, S., and Yeats, R. S., 1993, Paleomagnetic constraints on the initiation of uplift on the Santa Susana fault, western Transverse Ranges, California: Tectonics, vol. 12, p. 688-702.
Lewan, M. D., and Fisher, J. B., 1994, Organic Acids from Petroleum Source Rocks, in: Pittman, E. D., and Lewan, M. D., eds., Organic Acids in Geologic Processes: Berlin, Springer, p. 70-114.
Longstaffe, F. J., 1989, Stable Isotopes as Tracers in Clastic Diagenesis, in: Hutcheon, I. D., ed., Short Course in Burial Diagenesis: Toronto, Mineralogical Association of Canada, p. 201-277.
Lundegard, P. D., and Kharaka, Y. K., 1994, Distribution and Occurrence of Organic Acids in Subsurface Waters, in: Pittman, E. D., and Lewan, M. D., eds., Organic Acids in Geologic Processes: Berlin, Springer, p. 40-69.
Lundegard, P. D., and Land, L. S., 1986, Carbon Dioxide and Organic Acids: Their Role in Porosity Enhancement and Cementation, Paleogene of the Texas Gulf Coast, in: Gautier, D. L., ed., Roles of Organic Matter in Sediment Diagenesis: Tulsa, Society of Economic Paleontologists and Mineralogists, p. 129-146.
Luyendyk, B. P., 1991, A model for Neogene crustal rotations, transtension, and transpression in southern California: Geological Society of America Bulletin, vol. 103, p. 1528-1536.
MacKinnon, T. C., 1989, Petroleum Geology of the Monterey Formation in the Santa Maria and Santa Barbara Coastal and Offshore Areas, in: MacKinnon, T. C., ed., Oil in the California Monterey Formation: American Geophysical Union, Field Trip Guide Book T311, p. 11-27.
Malone, M. J., Baker, P. A., and Burns, S. J., 1994, Recrystallization of dolomite: evidence from the Monterey Formation (Miocene), California: Sedimentology, vol. 41, p. 1223-1239.
Matthews, A., and Katz, A., 1977, Oxygen isotope fractionation during the dolomitization of calcium carbonate: Geochimica et Cosmochimica Acta, vol. 41, p. 1431-1438.
Miller, N. R., 1995, Lithostratigraphic Signal Evaluation of the Miocene Monterey Formation, South Elwood Field, Santa Barbara-Ventura Basin, California [Ph. D. Thesis]: University of Dallas, Texas, 606 p.
Murata, K. J., and Larson, R. R., 1975, Diagenesis of Miocene Siliceous Shales, Temblor Range, California: U. S. Geological Survey Journal of Research, vol. 3, p. 553-566.
Murata, K. J., and Nakata, J. K., 1974, Cristobalitic Stage in the Diagenesis of Diatomaceous Shale: Science, vol. 184, p. 567-568.
Murata, K. J., and Randall, R. G., 1975, Silica Mineralogy and Structure of the Monterey Shale, Temblor Range, California: U. S. Geological Survey Journal of

Research, vol. 3, p. 567-572.

Murray, G. H. Jr., 1968, Quantitative Fracture Study – Spanish Pool, McKenzie County, North Dakota: AAPG Bulletin, vol. 52, p. 57-65.

Narr, W., 1991, Fracture Density in the Deep Subsurface: Techniques with Application to the Point Arguello Oil Field: AAPG Bulletin, vol. 75, p. 1300-1323.

Ogle, B. A., Wallis, W. S., Heck, R. G., and Edwards, E. B., 1987, Petroleum Geology of the Monterey Formation in the Offshore Santa Maria/Santa Barbara Areas, in: Ingersoll, R. V., and Ernst, W. G., eds., Cenozoic Basin Development of Coastal California: Englewood Cliffs, Prentice-Hall, p. 382-406.

Olson, D. J., 1982, Surface and subsurface geology of the Santa Barbara-Goleta metropolitan area, Santa Barbara county, California [M. S. thesis]: Oregon State Univ., 71 p.

Petersen, N. F., and Hickey, P. J., 1987, California Plio-Miocene Oils: Evidence of Early Generation, in: Meyer, R. F., ed., Exploration for Heavy Crude Oil and Natural Bitumen: AAPG Studies in Geology, vol. 25, p. 351-359.

Pisciotto, K. A., 1981, Diagenetic trends in siliceous facies of the Monterey Shale in the Santa Maria region, California: Sedimentology, vol. 28, p. 547-571.

Pisciotto, K. A., and Garrison, R. E., 1981, Lithofacies and depositional environments of the Monterey Formation, California, in: Garrison, R. E., and Douglas, R. G., eds., The Monterey Formation and Related Siliceous Rocks of California: Pacific Section Society of Economic Paleontologists and Mineralogists Special Publication, vol. 15, p. 97-122.

Pollastro, R. M., 1990, Geothermometry from Smectite and Silica Diagenesis in the Diatomaceous Monterey and Sisquoc Formations, Santa Maria Basin, California: AAPG Bulletin, vol. 74, p. 742.

Radke, B. M., and Mathis, R. L., 1980, On the Formation and Occurrence of Saddle Dolomite: Journal of Sedimentary Petrology, vol. 50, p. 1149-1168.

Redwine, L. E., 1981, Hypothesis Combining Dilation, Natural Hydraulic Fracturing, and Dolomitization to Explain Petroleum Reservoirs in Monterey Shale, Santa Maria Area, California, in: Garrison, R. E. & Douglas, R. G., eds., The Monterey Formation and Related Siliceous Rocks of California, SEPM Pacific Section, Los Angeles, p. 221-248.

Roehl, P. O., and Weinbrandt, R. M., 1985, Geology and Production Characteristics of Fractured Reservoirs in the Miocene Monterey Formation, West Cat Canyon Oilfield, Santa Maria Valley, California, in: Roehl, P. O., and Choquette, P. W., eds., Carbonate Petroleum Reservoirs: New York, Springer, p. 526-545.

Rosenbaum, J., and Sheppard, S. M. F., 1986, An isotopic study of siderites, dolomites and ankerites at high temperatures: Geochimica and Chosmochimica Acta, vol. 50, p. 1147-1150.

Seilacher, A., 1969, Fault-graded beds interpreted as seismites: Sedimentology, vol. 13, p. 155-159.

Sibson, R. H., 1996, Structural permeability of fluid-driven fault-fracture meshes: Journal of Structural Geology, vol. 18, p. 1031-1042.

Stearns, D. W., and Friedman, M., 1972, Reservoirs in Fractured Rock, in, King, R. E., ed., Stratigraphic Oil and Gas Fields: Classification, Exploration Methods, and Case Histories: AAPG Memoir, vol., 16, p. 82-106.

Stein, C. L., and Kirkpatrick, R. J., 1976, Experimental Porcelanite Recrystallization Kinetics: A Nucleation and Growth Model: Journal of Sedimentary Petrology, vol. 46, p. 430-435.

Surdam, R. C., and Crossey, L. J., 1985, Mechanisms of Organic/Inorganic Interactions in Sandstone/Shale Sequences, in: Gautier, D. L., Kharaka, Y. K., and Surdam, R. C., eds., Relationship of Organic Matter and Mineral Diagenesis: Society of Economic Paleontologists and Mineralogists Short Course No. 17, p. 177-232

Sylvester, A. G., 1995, Aseismic growth of the Ventura Avenue anticline (1978 to 1991): Evidence of anelastic strain release in Ventura basin, southern California: EOS, vol. 76, p. F141.

Taylor, H. P. Jr., 1979, Oxygen and hydrogen isotope relationships in hydrothermal mineral deposits, in: Barnes, H. L., ed., Geochemistry of Hydrothermal Ore Deposits, Second Edition: New York, Wiley, p. 236-277.

Ungerer, P., Behar, E., and Discamps, D., 1983, Tentative Calculation of the Overall Volume Expansion of Organic Matter during Hydrocarbon Genesis from Geochemistry Data. Implications for Primary Migration: Proceedings of the International Meeting on Organic Geochemistry (Advances in Organic Geochemistry 1981), vol. 10, p. 129-135.

Walther, J. V., and Helgeson, H. C., 1977, Calculation of the Thermodynamic Properties of Aqueous Silica and the Solubility of Quartz and its Polymorphs at High Pressures and Temperatures: American Journal of Science, vol. 277, p. 1315-1351.

Williams, L. A., Parks, G. A., and Crerar, D. A., 1985, Silica Diagenesis, I. Solubility Controls: Journal of Sedimentary Petrology, vol. 55, p. 301-311.

Wilson, J. C., and McBride, E. F., 1988, Compaction and Porosity Evolution of Pliocene Sandstones, Ventura Basin, California: AAPG Bulletin, vol. 72, p. 664-681.

Winter, B. L., and Knauth, L. P., 1992, Stable Isotope Geochemistry of Carbonate Fracture Fills in the Monterey Formation, California: Journal of Sedimentary Petrology, vol. 62, p. 208-219.

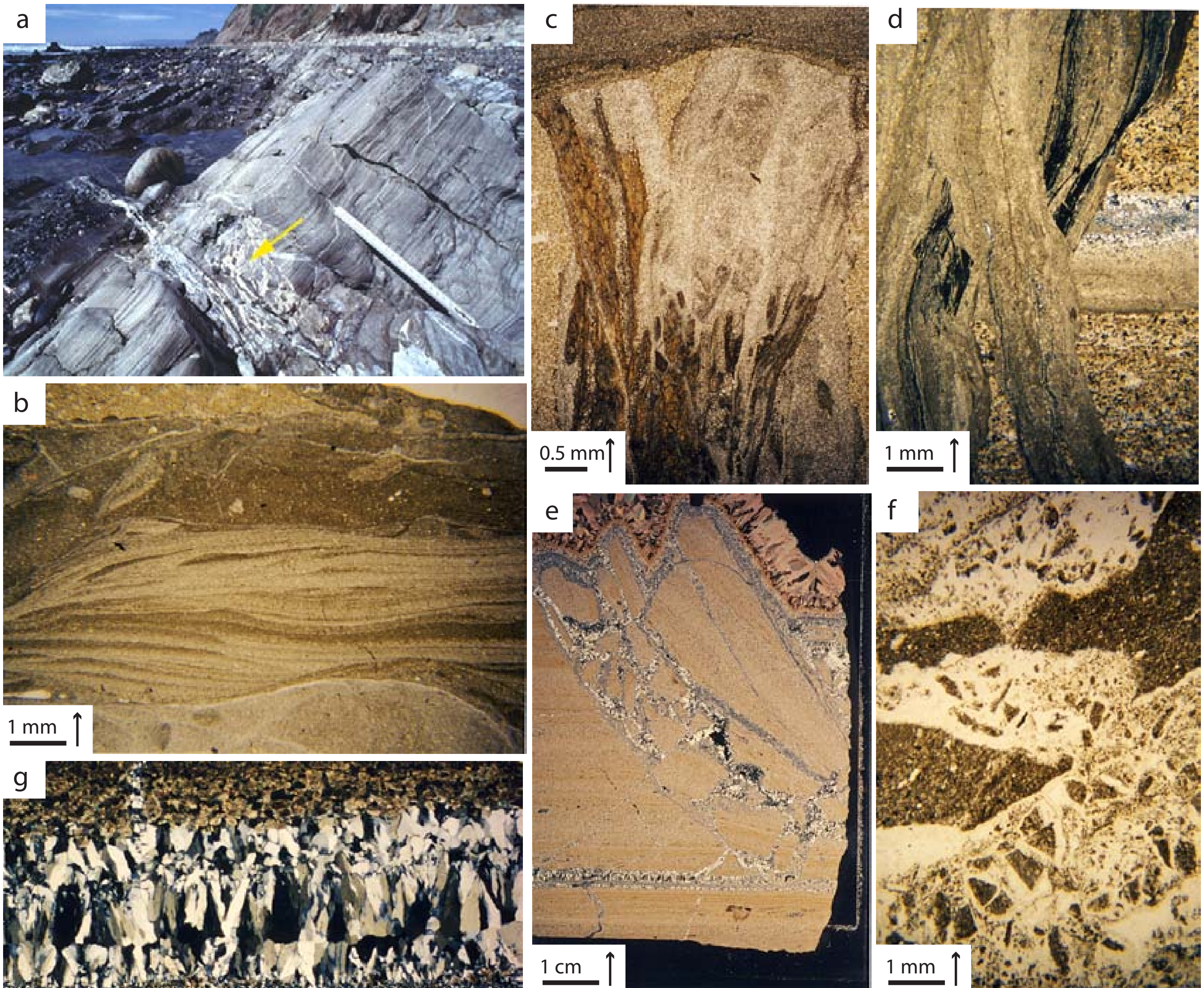

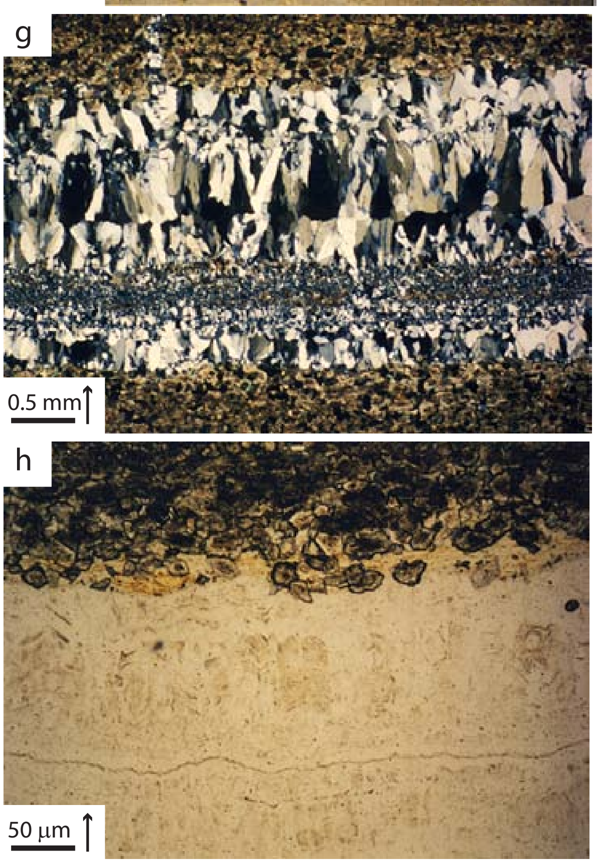

Plate 1. a. Dolomicrite F1 vein containing fragments of brecciated siliceous dolostone. Stratification of dolomicrite vein fill (arrow) is parallel to bedding indicating vein filling prior to regional folding and tilting of bedding by 55°. F1 dolomicrite veins are partly reactivated by F4 calcite veins that extend into over- and underlying mudstone. Scale is 22 cm. Arroyo Burro Beach. b. Cross-bedded and graded laminae of dolomicrite in sub-horizontal F1 vein in dolostone bed at Ellwood Beach. Grading indicates transport and deposition of micrite as detrital material in flowing fluid. Arrow points up. c. Laminae of organic-rich siliceous dolomicrite (dark colored), in part recrystallized (light colored). Elongate patches of unrecrystallized dolomicrite suggest that recrystallization was aided by percolation of fluid through the micrite, removing portion of the organic material. Ellwood Beach. Arrow points up. d. Mutual crosscutting of dolomicrite laminae in F1 vein. Dolomicrite contains cryptocrystalline quartz which is isotropic (black) in cross-polarized light. Arroyo Burro Beach. Arrow points up. e. Bedding parallel quartz-cemented breccia. Fragments are slightly displaced in lower part of breccia but rotated and translated in upper part. Geopetal layers of microcrystalline quartz are deposited on top of fragments (e.g. fragment on upper left). Top cavity is subsequently cemented with dolomicrite and bladed calcite. Late calcite is in part replaced by quartz and hydrocarbons. Arroyo Burro Beach. Arrow points up, cross-polarized light. f. Dissolution of dolomite and replacement by quartz (clear) in F2 breccia. Dolomite of initially siliceous dolostone is dissolved by surface corrosion of fragments (e.g. large fragment in center) and by corroding dolomite in the matrix leading to disaggregation of siliceous dolostone. Arroyo Burro Beach. Arrow points up. g. Geopetal layer of microflamboyant quartz in F2 quartz vein. Layer was deposited after partial cementation of vein by columnar quartz. Arroyo Burro Beach. Arrow points up, cross-polarized light. h. Corrosion of siliceous dolostone and replacement by inclusion-rich quartz along margin of F2 quartz vein. Host dolomite recrystallized in part to inclusion-free dolomite rhombs, forming inclusions in quartz. Fine organic inclusions in lower, more central, part of quartz vein outline idiomorphic crystal terminations indicative of growth into open space. Detail of g. Arrow points up.

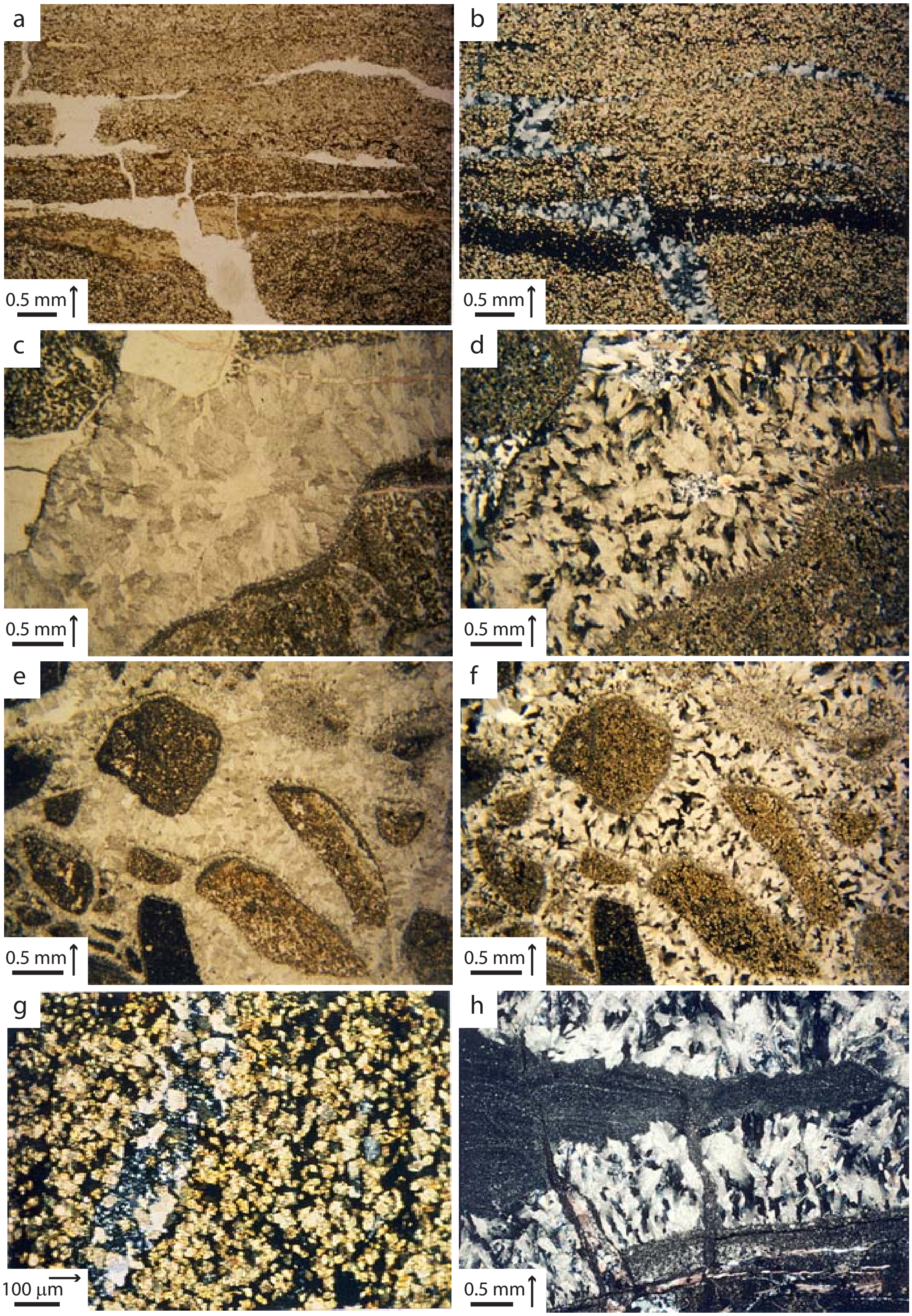

Plate 2. a. Incipient fragmentation during F2 fracture formation, concurrent with opal-CT dissolution–quartz precipitation in siliceous dolostone. Arroyo Burro Beach. Arrow points up. b. Same as a., cross-polarized light. Note initiation of fractures in organic rich opal-CT layer. Opal-CT is pseudo-isotropic. c. Breccia fragments of siliceous dolomite and of F2 quartz vein fill are cemented by F3 dolomite cement. Detrital dolomicrite forms veneer on fragments. Late F4 fractures and residual breccia cavity (center) are cemented by calcite and quartz. Arroyo Burro Beach. Arrow points up; plane-polarized light. d. Fanning columnar crystals with sweeping extinction and curved crystal faces are characteristic of baroque dolomite. Same view as d, cross-polarized light. e. Varying stages of recrystallization and replacement of siliceous dolostone breccia fragments. Opal-CT (dark) is dissolved while dolomite recrystallizes. Note dolomicrite layers on top of breccia fragments. Arroyo Burro Beach; Arrow points up. f. Same as e., cross-polarized light. g. Microflamboyant quartz in pore of opal-CT-containing dolostone, indicating that opal-CT (isotropic) is unstable during F2 quartz vein formation. Detail of a. Arrow points up; cross-polarized light. h. Stratified dolomicrite in residual cavity after baroque dolomite vein precipitation. Stratification is parallel to bedding of the host rock. Arroyo Burro Beach. Arrow points up.

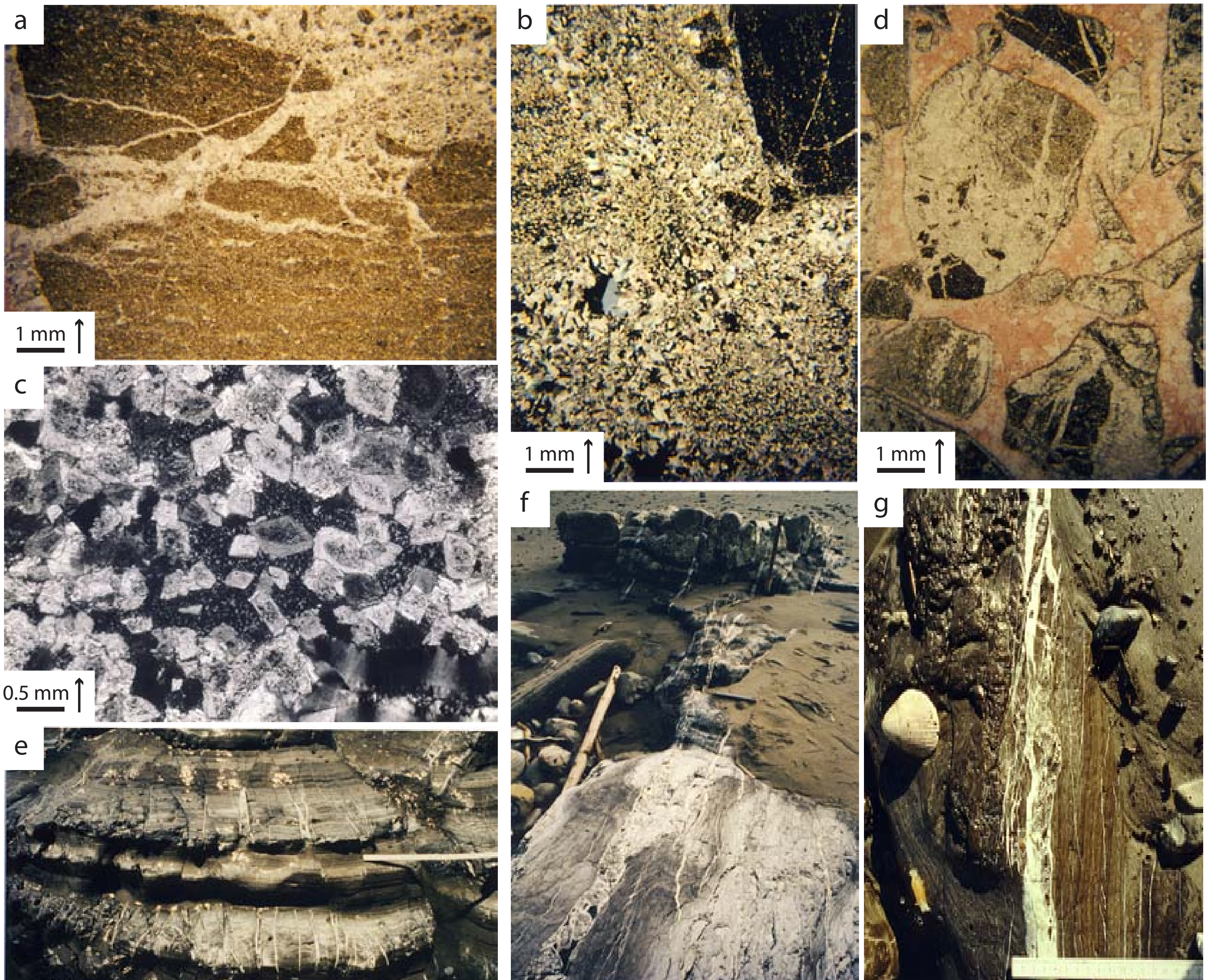

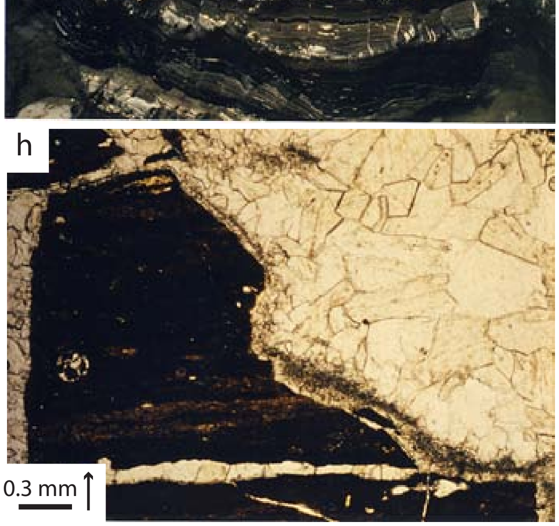

Plate 3. a. Fragments of dolostone rich in organic inclusions recrystallize to a mosaic of equant, inclusion-free dolomite (top right), similar to vein-filling baroque dolomite at bottom left. Arroyo Burro Beach. Arrow points up; plane-polarized light. b. Fragments of dolomitic opal-CT porcelanite show varying amounts of dolomite recrystallization and replacement of opal-CT by dolomite. Opal-CT is pseudo-isotropic (dark). Heavily replaced fragments contain only little diagenetic microcrystalline silica indicating dissolution and transfer of silica out of the section. Silica may be deposited upsection as F2 quartz vein cement. Some late quartz cement postdating dolomite is seen in center part of the section. Arroyo Burro Beach. Arrow points up; cross-polarized light. c. Silica-rich lamina in siliceous dolostone contains rhombs of inclusion-poor dolomite which appear to postdate microflamboyant quartz, but clearly predate chalcedony in pore space (top right). Arroyo Burro Beach. Arrow points; cross-polarized light. d. Rebrecciated dolomite (F3) breccia, cemented by calcite (stained). Micritic calcite forms geopetal layer on top of breccia components. Note varying degree of dissolution and replacement by dolomite of originally dolomitic opal-CT porcelanite. Arroyo Burro Beach. Arrow points up. e. Calcite veins in porcelanite layer at Arroyo Burro Beach. The extensional strain of these veins is accommodated in the under-and overlying mudstone beds by conjugate sets of normal faults. Scale is 1 cm wide. f. Calcite cemented 'breccia veins' cut across dolostone (top), mudstone (middle), and porcelanite (foreground) with varying thickness depending on host lithology, 10 m east of fault at Arroyo Burro Beach. g. Clustering of veins and the formation of cross-fractures leads ultimately to host rock brecciation. h. Calcite micrite blankets the corroded top surface of a host rock fragment in a calcite cemented F4 breccia. Arroyo Burro Beach. Arrow points up.

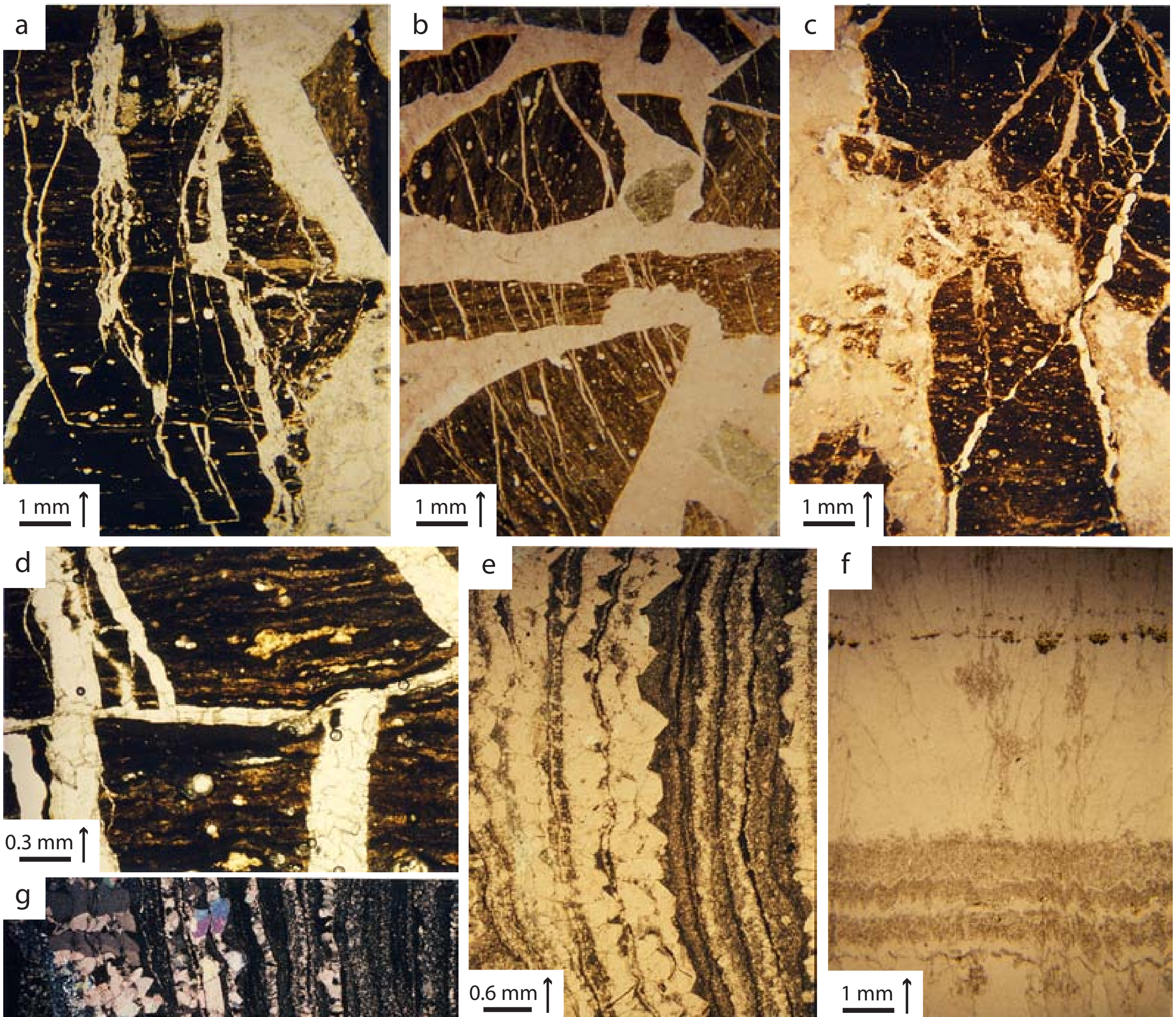

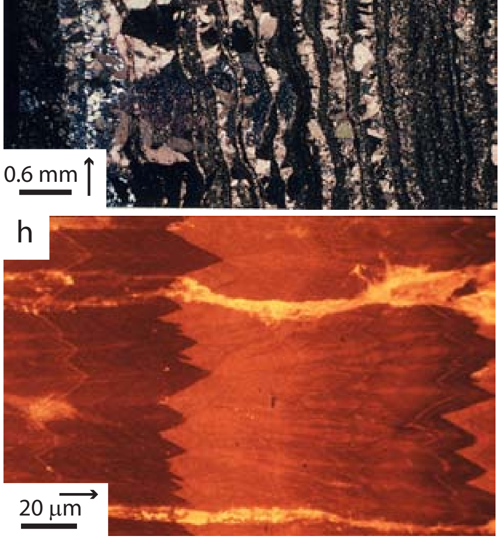

Plate 4. a. Fragmented opal-CT porcelanite, cemented by calcite. Compared to earlier F2 (quartz) and F3 (dolomite) cemented breccias, the host rock less dissolution and replacement but intense fragmentation. Arroyo Burro Beach. Arrow points up. b. Fragments of opal-CT porcelanite and dolostone are locally corroded. Corroded fragment in center and uncorroded fragment to the right are of similar composition suggesting that localization of corrosion is controlled by surface effects such as wetting differences of oil versus water. Later veins cut across fragments and earlier calcite cement. Arroyo Burro Beach. Arrow points up. c. Corrosion and disintegration of organic-rich opal CT porcelanite fragment in fine breccia, filling F4 vein at Arroyo Burro Beach. Latest veins were filled with bitumen which is largely replaced by epoxy during section preparation. Arrow points up. d. Calcite-cemented veins in same sample as a. Seams of host rock outline the margin of the central horizontal vein, indicative of crack-seal vein formation. Vein contact at lower left is lined with bitumen, largely replaced by epoxy. Bitumen suggests that last crack-opening increment was invaded by bitumen before calcite cementation. Arrow points up. e. Laminae of micrite fill topography of idiomorphic calcite crystal terminations, suggesting growth of bladed calcite into open fracture space and deposition of micrite as detrital material. Detail of g. Arrow points up. f. Bands of single-phase aqueous (bottom) and solid (top) inclusions alternate with inclusion-poor layers in 10-20 cm thick botryoids of bladed calcite along the fault at Arroyo Burro Beach. Arrow in growth direction. g. Alternating layers of bladed and micritic calcite cement with partial replacement by quartz in vertical vein. Despite the disruption in precipitation of bladed calcite by micrite, the bladed calcite retains its optical continuity. Arrow points up; cross-polarized light. h.: Alternating bands of luminescent and non-luminescent calcite in banded fault calcite cement at Arroyo Burro Beach. Luminescence bands are about 100 µm thick. Arrow in growth direction.